AERODYNAMIC ANALYSIS OF FLAPPING WING MICRO AIR VEHICLES

By

HALEEMA ZAREEN

2009-NUST-MS-PhD-Mech-09

MS-60

Submitted to the Department of Mechanical Engineering in Fulfillment of the Requirements for the Degree of

MASTER OF SCIENCE

in

MECHANICAL ENGINEERING

Thesis supervisor

Dr. M. Afzaal Malik

College of Electrical & Mechanical Engineering

National University of Sciences & Technology

2013

Acknowledgements

All praise to Allah Almighty for bestowing me with the courage, knowledge and health to carry out this project.

I would like to thank my beloved parents and family, who prayed for me, their endless effort and support made it possible for me, to be, what I am today.

I am extremely grateful to Dr. M. Afzaal Malik who allowed me to work under his supervision. He has been very helpful and supportive. He always encouraged me and boosted my moral whenever I was depressed. Without his guidance and persistent help, this dissertation would not have been possible.

A sincere gratitude to my committee members Dr. Hossein Raza Hamdani, Dr. Syed Waheed ul Haq, Dr. Imran Akhtar and Raja Amer Azeem for their supervision in my academic endeavours.

My special thanks to Dr. Hossein Raza hamdani who helped, supported and guided me whenever I faced difficulty in my research work.

I would like to acknowledge my dear friends Nida Ahsan, Sana Mahmood Awan and Shafia kausar for always being there for me. I will not forget to acknowledge the role of Muhammad Nafees Mumtaz Qadri in learning the softwares and discussing various problems that arose during the course of time.

In the end I would like to thank the entire honorable faculty of Mechanical Department of the College of Electrical and Mechanical Engineering to be so supportive.

Declaration

I hereby declare that I have developed this thesis on the basis of my personal efforts under the sincere guidance of my supervisor Dr. M. Afzaal Malik. All the sources used in this thesis have been cited and the contents of this thesis have not been plagiarized. No portion of the work presented in this thesis has been submitted in support of any application for any other degree of qualification to this or any other university or institute of learning.

_____

Haleema Zareen

TABLE OF CONTENTS

LIST OF FIGURES

List of Tables

ABSTRACT

Micro air vehicle (MAV) is defined as unmanned air vehicles with wing to wing span of 15 cm and weight not more than 100 grams, specifications defined by American Defense Advanced Research Projects Agency (DARPA). MAV finds its applications in surveillance, rescues and other strategic military purposes. The design of a Micro air vehicle (MAV) is an emerging new area of current research. Especially, the problem of aerodynamic behavior of the flapping wing of an mav is a very challenging problem for researchers. It is particularly helpful for design and development of Micro Air Vehicles where optimized lift and thrust generation is very much required. In the present research, the impact of airfoil shapes on the flapping performance has been investigated by comparing the lift and drag coefficients by using three different airfoils which include flat plate, ellipse and NACA0014 of same thickness in pure plunging motion. Computations were carried out at various Reynolds number that cover entire spectrum from fully laminar to fully turbulent flow regime and at various reduced frequencies in order to explore behavior of different shapes of airfoils and their correlation with Reynolds number and reduced frequencies. Unsteady incompressible Navier Stokes equations in this study were solved assuming flow to be laminar at low Reynolds number whereas for high Reynolds S-A turbulence model has been used to carry out computations. O-type grid has been used to descretize the computational domain. Results obtained show that the airfoil shape has strong influence on flapping performance and its correlation with the Reynolds number and reduced frequency has also been found which leads to the conclusion that at high Reynolds number and for higher reduced frequencies, shaped airfoils that is NAC0014 produces best thrust.

Chapter 1: INTRODUCTION

1.1 MOTIVATION

Defense Advance Research Project Agency (DARPA) has defined MAVs as vehicles having a span of 15cm, weight of 50gms and a flight speed of 15-20 m/sec. These types of vehicles have advantages of small size and have applications in surveillance, reconnaissance, targeting and sensing purpose [1, 2]. MAVs can be broadly categorized into three types that is Fixed wing MAVs, Rotary wing MAVs and Flapping wing MAVs as shown in figure 1-1, 1-2 and 1-3 respectively. Fixed wing MAVs are efficient but they lack the ability to hover and hence not suitable for application confined in space [1, 3]. Rotary wing MAVs are able to hover but they are less efficient than Fixed Wing MAVs [3]. When the MAVs scale is below 15cm with the conventional layout fixed wing it cannot obtain enough lift to drag ratio and unable to fly at low Reynolds number [4]. Therefore, flapping wing MAVs can be used which provide high lift to drag ratios as compared to fixed wings MAVs.

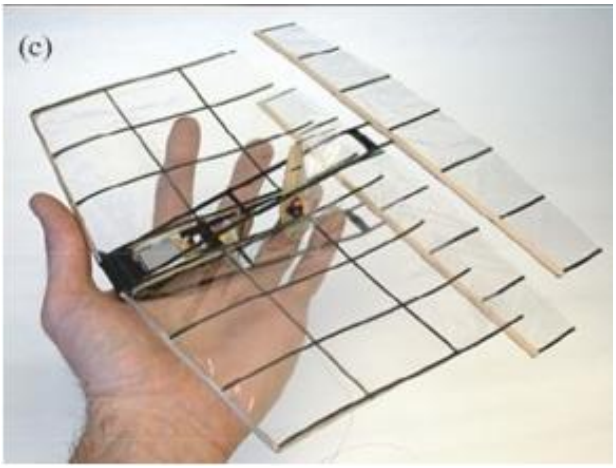

Figure 1-1 Fixed Wing Micro Air Vehicle [1]

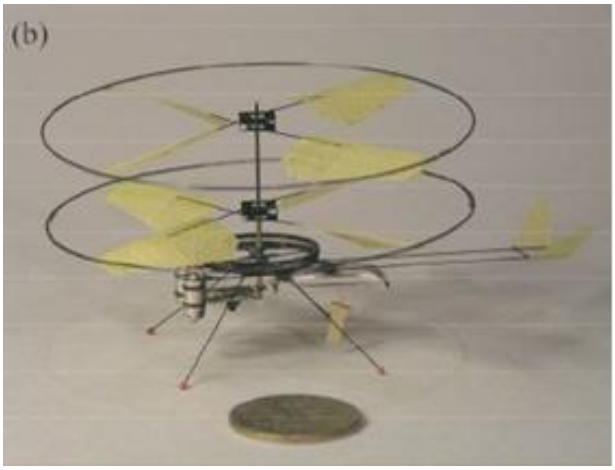

Figure 1-2 Rotary wing Micro Air Vehicle [1]

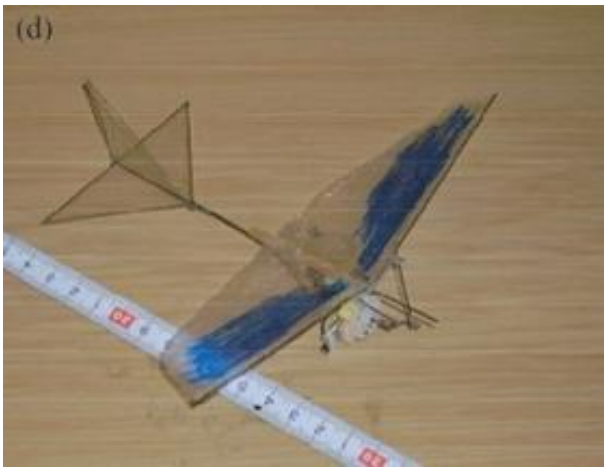

Figure 1-3 Flapping wing Micro Air Vehicle [1]

MAVs usually operate in a low Reynolds number regime of $10^3 – 10^5$ which is about the same at which large insects and small birds operate [1]. So it may be beneficial to take inspiration from natural flyers to learn their flight physics because fixed wing aircrafts, helicopters and propellers become less efficient as the speed and the size decreases which also causes the Reynolds number to decrease. This is because the viscous forces increase which causes thicker boundary layer to form and flow separation causes loss of lift and increased pressure drag [5]. Flapping wings are now being actively studied because they provide greater efficiencies even at low Reynolds number. In this range of low Reynolds number, MAVs like birds and insects achieve flight by flapping their wings which results in unsteady aerodynamics. This concept of flapping wing is actually motivated by observation of the flight

of birds and insects, which use various mechanisms not only to overcome the difficulties of low Reynolds number, but to exploit the associated aerodynamic phenomena. Traditional aircraft design uses fixed wing attempts to ensure that the flow remains attached to the airfoil (unstalled) all the times whereas these natural mechanisms that is flapping motion rely on the vortices (low pressure regions) that separate from the leading and trailing edges of the wings, which are responsible to create much higher lift and thrust than is possible with fixed wings [5].

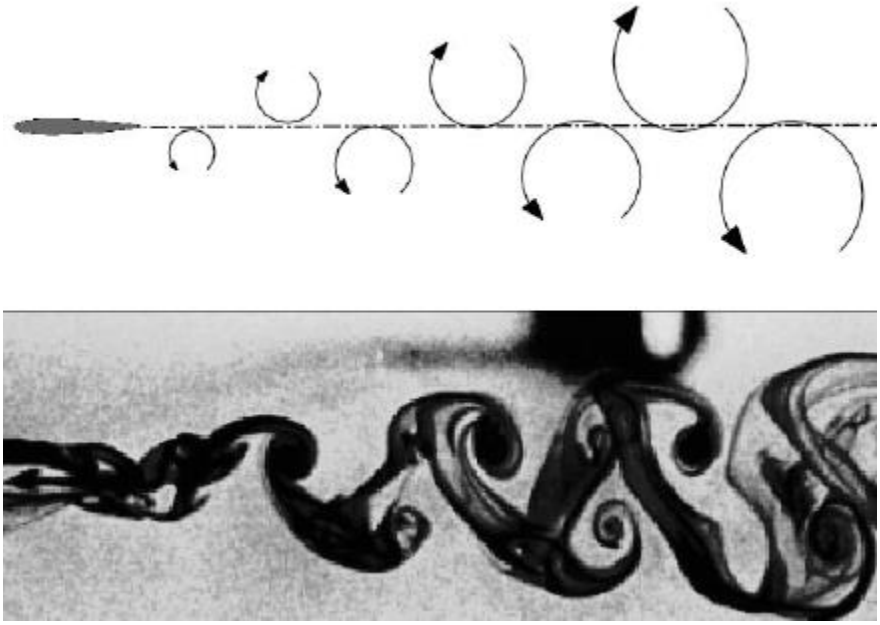

Figure 1-4 Von Karman Street indicative of drag [8]

In order to gain insight of flow physics that is the formation of leading and trailing edge vortices, the manner in which the vortices interact with the airfoil and themselves, how they contribute to lift, thrust and propulsion, various experiments and computational studies have been carried out. Birnbaum [6] observed the condition that leads to thrust generation when an incompressible air is made to pass over plunging airfoil. He suggested that the sinusoidal flapping (plunging) airfoil can be an alternative to conventional propeller and also beneficial for designing MAVs due to thrust generation along with high lift production. In 1930s Von Karman and Burgers [7] gave the theoretical explanation of thrust and drag produced by the airfoils based on the orientation of vortices observed in the wake of the airfoil. They observed

that two rows of counter rotating vortices in the wake could produce thrust on an airfoil in an incompressible flow which differs from the wake that is produced in case of stationary airfoil. When the flow is made to pass over the stationary airfoil at low Reynolds number, Von Karman Street is observed in the airfoil wake in which upper row consists of clockwise vortices and the lower row consists of counter clockwise vortices as shown in figure 1-4. This type of wake is momentum deficit and produces drag.

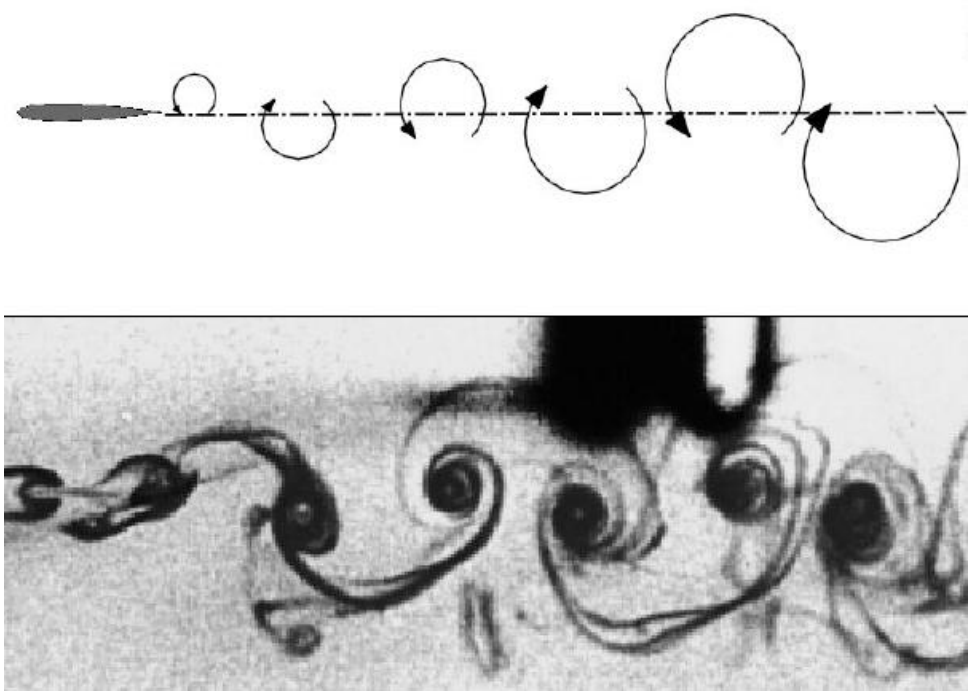

Figure 1-5 Reverse Von Karman Street indicative of thrust [8]

However, a sinusoidally oscillating airfoil generates a vortex street behind an airfoil which depends on the plunge velocity of an airfoil. Hence the vortex behind an oscillating airfoil can be drag indicative or thrust indicative in which the upper row consists of counter clockwise vortices and the lower row consists of clockwise vortices as shown in figure 1-5. This type of Vortex Street is known as Reverse Karman Vortex Street. Their work showed that the oscillating airfoil is capable of producing satisfactory amount of thrust.

1.2 OBJECTIVE

The main aim of the present research is to investigate the thrust production of 2-D airfoils in pure plunging motion at various conditions which include

i. Different airfoil shapes

ii. Different Reynolds number valid for small aerial vehicles

iii. Different reduced frequencies

Different shapes of airfoils have been used to explore the effect of shape of the airfoils on thrust production. Similarly, Reynolds number has also been varied to see the persistence of reverse vortex shedding over a range of Reynolds number valid for small aerial vehicles and the systematic investigation of reduced frequencies has also been carried out in order to see the Reverse vortex shedding for the intensity of unsteadiness. Computations has been performed by systematically varying the Reynolds number from a laminar regime (i.e 1000) to partially turbulent/transition regime (10,000) and then to fully turbulent (25,000). The values of reduced frequencies that have been used lie well in the range for biological flyers. Simply speaking, we are systematically investigating the plunging motion whose severity is determined by the reduced frequency (k) and then at a given Reynolds number to see the effect of change of shape on thrust production. Basically the objective is to give better explanation of thrust production of the airfoils in pure plunging motion at the above mentioned conditions and systematically arranging them to see their effect on thrust production.

1.3 THESIS OUTLINE

Brief outline of the whole thesis is described below

- Chapter one describes the brief overview and motivation on which the present research is carried out.
- Chapter two consists of detailed literature review describing experimental and numerical studies conducted on the airfoils in pure plunging motion.
- Chapter three covers the details of airfoil geometry and the computational setup that is used to carry out the numerical simulations. Commercial CFD package Fluent has been used to solve the 2D Navier Stokes equation.

- Chapter four consists of validation and sensitivity studies which include grid independence and domain independence that were performed to prove the independence of the numerical solver. It also covers the time step and turbulence model sensitivity studies.
- Chapter five comprises of the systematic investigation of effect of different shapes of airfoils on thrust generation at various reduced frequencies at Reynolds number of 10,000.
- Chapter six and seven cover the details of thrust generation of three different shapes of airfoils at Reynolds numbers of 1000 and 25,000.
- Chapter eight concludes the overall study carried out throughout the course of research work. A qualitative and critical analysis for all the cases discussed in the previous chapters will be carried out and summarized.

Chapter 2: LITERATURE REVIEW

Knoller [9] and Betz [10] were the first to describe the change of effective angle of attack of an oscillating airfoil which results in the generation of normal force component having both lift and thrust component. This phenomenon is known as knoller - Betz effect as shown in figure 2-1. They were the first to observe the unsteady flow dynamics of flapping wings.

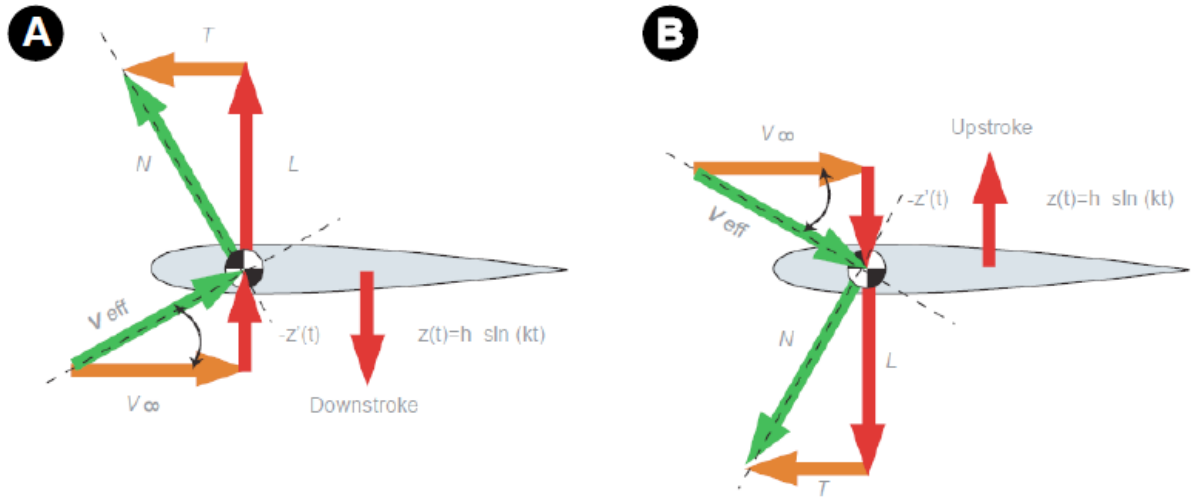

Figure 2-1 Lift (L) and Thrust (T) components of normal force vector (N) of airfoil in pure plunging motion [6]

Katzmayer [11] verified the knoller – Betz effect by placing stationary airfoil in wind tunnel having a sinusoidal oscillating wind stream and measured the average thrust. Flow physics and the effect of flapping parameters on thrust generation have been investigated numerically by using unsteady panel method and Navier Stokes equation during past decade.

Ashraf et al [12] reviewed the progress of CFD on flapping wing aerodynamics. They analyzed the effect of amplitude, non dimensional flapping velocity and reduced frequencies on thrust generation and efficiency of plunging airfoil at Re = 20,000. Computations were performed using NACA0012. Results agreed very well with the published data [13]. They also

found that very high values of thrust coefficient are obtained at K = 2.0 and h = 24. But the efficiency comes out to be very low at the same conditions.

Tuncer and Platzer [14] computed the unsteady, viscous low speed flow over NACA0012 in pitching/plunging motion at various reduced frequencies, amplitudes and phase shifts. Navier Stokes solver has been used for this purpose. They identified the flow separation and thrust producing vortices are found to be in good agreement with the water tunnel experiments. They concluded that high thrust can be obtained when the airfoil is made to plunge at higher frequencies in the presence of large leading edge vortices but the propulsive efficiency becomes significantly low. However in case of combined pitch and plunge motion, high propulsive efficiency along with high thrust production can be obtained because the flow remains attached to the airfoil.

Miao and Ho [15] explored the effect of span wise flexure amplitude on the aerodynamic performance of flapping airfoil at various Reynolds number and reduced frequencies. Flow was assumed to be viscous and computed for plunging airfoil. Flexure amplitude was varied from 0 to 0.7 with the interval of 0.1. They found that the thrust indicative wake is produced for flexure amplitude less than 0.5 of chord length. Also there is an increase in propulsive efficiency for flexure amplitude of 0.3. They also calculated thrust and propulsive efficiency at various Reynolds numbers and reduced frequencies and came to conclusion that propulsive efficiency is strongly correlated to reduced frequency.

Liangyu Zhao and Shuxing Yang [16] also investigated the effect of airfoil thickness on aerodynamic performance of the airfoil in pure plunging motion. Studies were performed from NACA0002 to NACA0020. Figure 2-2 represents these profiles with thickness varying from 2% to 20%.

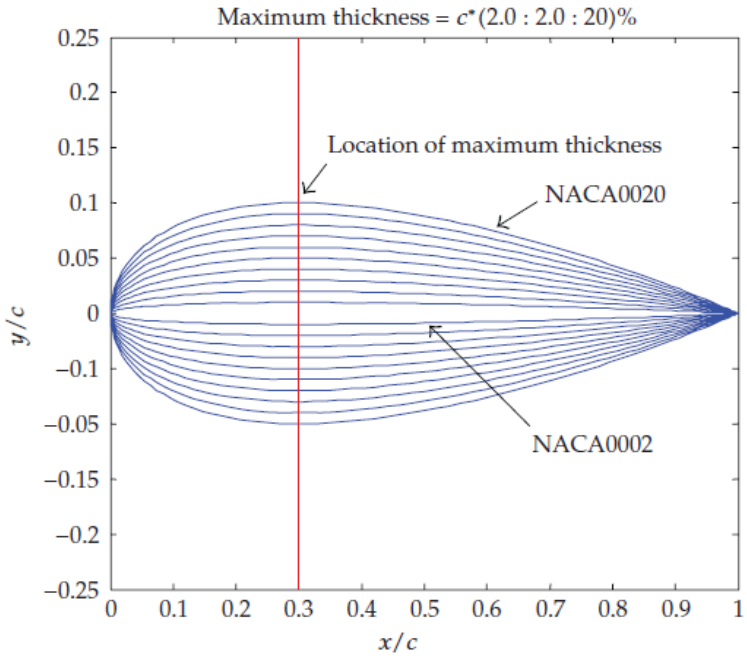

Figure 2-2 Profiles of NACA airfoil with varying thickness [16]

They observed that increase of the thickness of the airfoil results in increasing time averaged thrust coefficient and propulsive efficiency. This increasing trend was found to be linear upto a thickness value of about 12%. After this value, the effect of thickness is not much pronounced. Also the lift plots are identical for all the airfoils. Figure 2-3 represents the plot showing the variation of the thrust and propulsive efficiency due to change of the thickness of the airfoil.

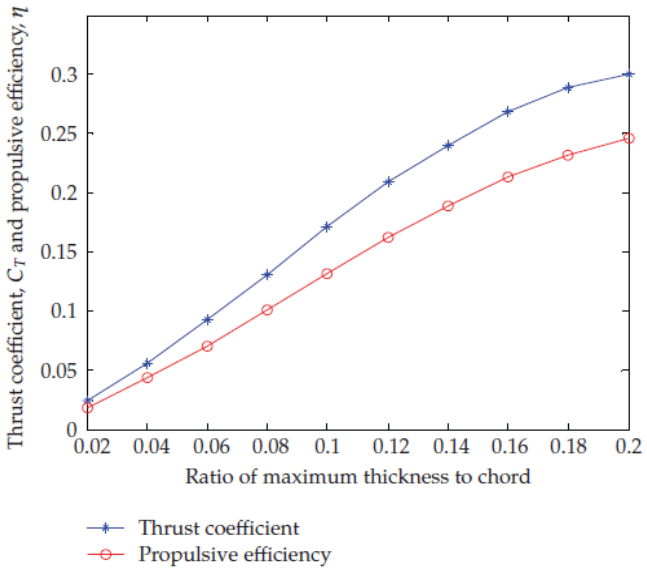

Figure 2-3 C_T and η versus maximum thickness [16]

They found that the increase of thickness of the airfoil reduces the strength of Leading Edge Vortex (LEV) and also its shedding is delayed. Hence thrust and propulsive efficiency of airfoil increases without reduction in lift. They also investigated the impact on lift, thrust and propulsive efficiency by varying the location of maximum thickness of the airfoil. Figure 2-4 shows the geometries of airfoil with maximum thickness location. As the point of maximum thickness is moved towards the leading edge, there is an increase in thrust and propulsive efficiency of airfoil as shown in figure 2-5 whereas there is no change in the lift coefficient.

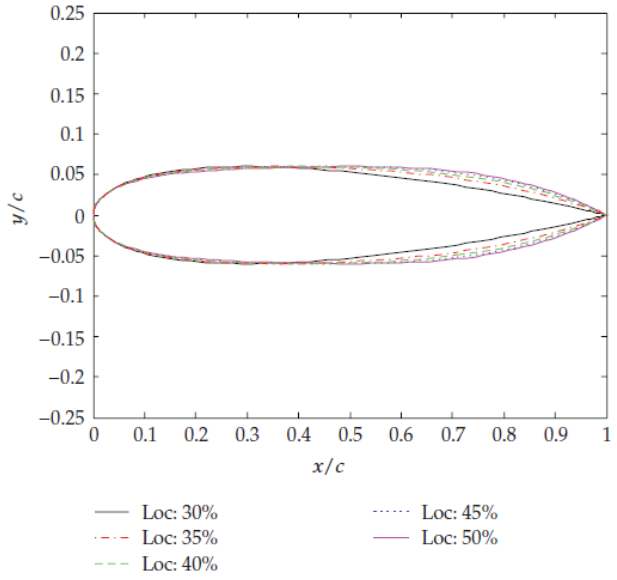

Figure 2-4 Airfoil shapes with different location [16]

Ashraf [17] numerically investigated the effect of airfoil thickness and camber effect on the propulsive efficiency and thrust generation of an airfoil in the Reynolds number range of 200-20×10^6. The study was performed using NACA series airfoils with thickness varying from 6% to 50%. Only seven airfoil sections of thickness 6%, 12%, 15%, 20%, 30%, 40% and 50% were used. Computations were performed at reduced frequency of K = 2.0 and plunging amplitude of h = 0.25 and 0.5. For pure plunging motion, computations were carried out reduced frequency K = 2.0 and plunge amplitudes of h = 0.025 and 0.5 and for pitching/ plunging motion at h = 0.5 and θ = 15° and 30°. Decrease in thrust and propulsive efficiency is observed with the increase in thickness of airfoil upto some critical value of thickness for

Reynolds number (Re) = 200 as shown in figure 2-6 because more rounder leading edge weakens the suction peak.

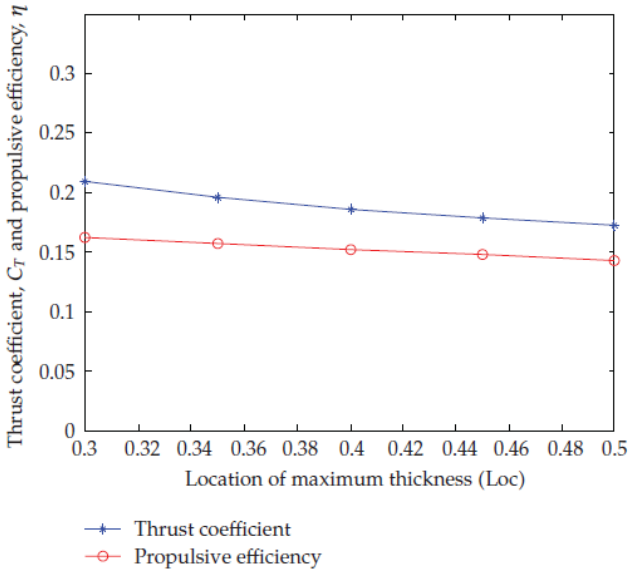

Figure 2-5 Trends of C_T and η versus Loc [16]

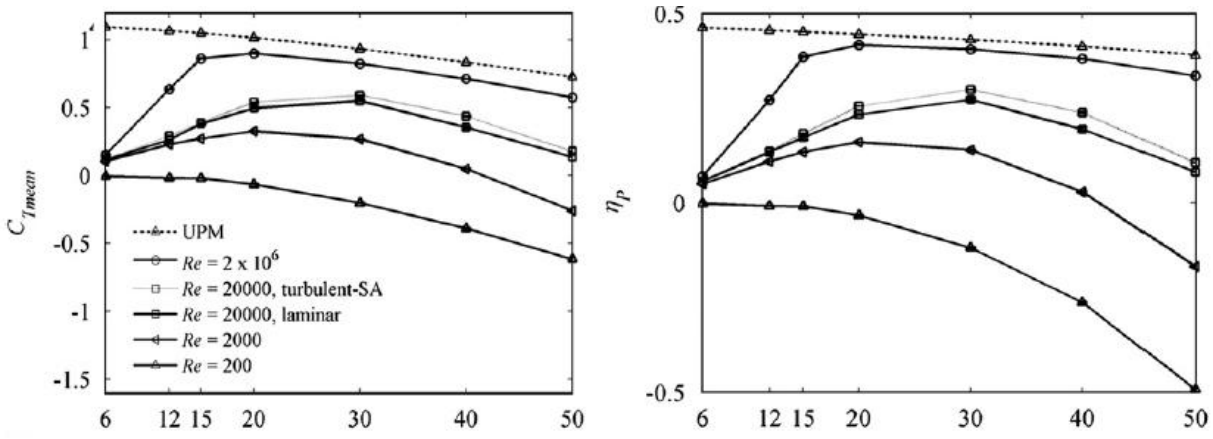

Figure 2-6 C_{Tmean} and η variation with the thickness of plunging airfoils [17]

At high Reynolds number, thrust and propulsive efficiency increases with the increase of thickness of the airfoil. Performance of airfoil was also checked by varying camber location at Reynolds number of 2000. Little variation in thrust was found by varying camber location.

Guerrero [18] carried out the parametric study to explore the effect of cambering on aerodynamic performance of the airfoils in heaving motion. Airfoils were assumed rigid and

incompressible Navier Stokes equation was employed to carry out computations. For this purpose, numerical computations were performed at Reynolds number equal to 1100 and at different reduced frequencies and strouhal numbers. It was observed that time averaged lift coefficient is strongly affected due to variation of airfoil camber in heaving motion whereas the change in time averaged thrust coefficient and propulsive efficiency is not much pronounced.

Wen and Liu [19] studied the mechanism of thrust generation for viscous flow past airfoils in plunging motion by discussing the contribution of pressure and viscous forces. Computations were carried out by varying thickness of elliptic airfoils and also for different shapes of airfoils. They observed that for ellipse having 1% thickness, viscous forces are responsible for thrust generation whereas pressure forces can be ignored from Reynolds number 50-5000. With the increase of thickness of airfoil, thrust changes to drag as shown in figure 2-7.

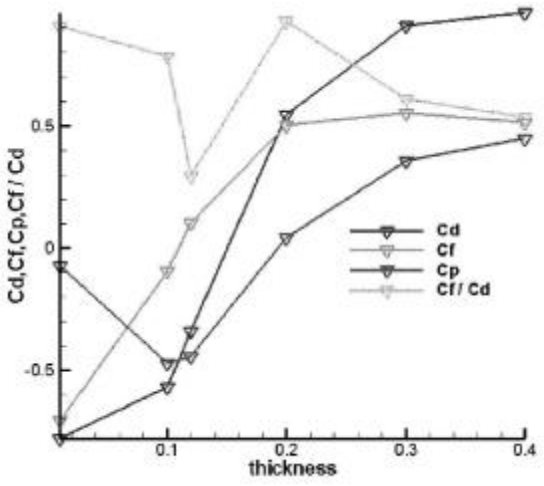

Figure 2-7 Variation of various aerodynamic coefficients Vs thickness of ellipse [19]

Flow was also simulated on different shapes of airfoils having same thickness at Reynolds number of 100. NACA0012, elliptic and reverse NACA0012 have been considered. The results showed that NACA0012 produces largest amount of thrust as

compared to other two airfoils. The values of coefficient of drag of the three shapes are given in table 2-1.

Table 2-1 The drag Coefficient of different airfoils (Re=100) [19]

Airfoil	Re = 100		
	C_d	C_{df}	C_{dp}
NACA0012	-1.17	0.27	-1.44
Ellipse	-0.34	0.1	-0.44
Reverse NACA0012	0.36	0.52	0.87

Young and Lai [20] investigated the effect of amplitude and frequency in the wake of plunging airfoils. Flow past the plunging airfoil was computed by using incompressible Navier stokes equation at Reynolds number of 30,000. It is observed that there is a close agreement between the numerically computed wake structures with that obtained in the experiments. They also concluded that the wake produced by the plunging airfoils strongly depends on both the strouhal number and reduced frequency at the given Reynolds number.

Young and Lai [21] carried out a comparison of aerodynamic forces produced by plunging NACA0012 at Reynolds number of 20,000 by using Navier Stokes code was made with that of UPM (unsteady panel mehod) and Garrick analysis. UPM and Garrick analysis predict that aerodynamic forces increase with the increase of *Kh* but have little variation with increase of reduced frequency *K*. This is because the two codes are based on kutta condition and does not allow flow separation. However Navier stokes predicted that aerodynamic forces are a strong function of reduced frequency. It was also concluded that the frequency dependence is due to the shedding of vortex from the leading edge of the airfoil. Large amount of thrust is produced by the airfoil at high values of reduced frequencies because of the formation of another leading edge vortex on the opposite side of the airfoil as the previous vortex is not convected far downstream. At lower values of *K*, propulsive efficiency

is reduced because the vortex travels far downstream over the airfoil surface which results in drag production for a larger portion of the plunge cycle.

T. Benkherouf a, M.Mekadem [22] explored the effect of flapping frequency on the flow physics of the self-propelled flapping airfoils. Simulations were carried out using NACA0014. In this research, no velocity was set at inlet flow. Flapping frequency was varied from 0.1 to 20 Hz for plunging amplitudes of 10%, 17.5%, 25% and 40%. It was observed that the propulsion velocity found to increase with both the flapping amplitude and frequency.

Above discussion shows that most of the studies related to geometry of the airfoil were carried out by varying the thickness of the same type of airfoil showing that change in the thickness of the airfoil results in change of geometry of airfoil which affects the aerodynamic force coefficient that is thrust coefficient of the airfoil. A very few studies were conducted to compare the aerodynamic performance of different shapes of airfoils in plunging motion. Wen and Liu [19] compared the aerodynamic performance of three different shapes of airfoils as discussed previously but their research was only focused on the thrust generation of different shapes of airfoils at $Re = 100$. In addition, studies were also conducted to see the effect of variation of reduced frequency and plunge amplitude at some particular Reynolds number on the thrust generation of the airfoil by investigating the flow physics. Afore mentioned studies shows that the aerodynamic performance of different shapes of airfoils has not been explored enough.

In the present research, comparison of lift and thrust generation of different shapes of airfoils has been carried out at various Reynolds numbers that covers the entire spectrum from fully laminar to fully turbulent regime and then by varying the flapping frequency at the given Reynolds number (that lie in fully laminar, laminar to turbulent and fully turbulent flow regimes) in order to have the real insight of the variation in the lift and thrust coefficient

due to change in airfoil geometry and to explore the correlation of the change of geometry of airfoil with the Reynolds number and flapping frequency of the airfoil.

Chapter 3: COMPUTATIONAL SETUP

3.1 PHYSICAL MODEL

The present study focuses on the airfoils in pure plunging motion. Therefore, in order to simulate the plunging motion, the flow field around the airfoil is modeled in two dimensions with the axis of airfoil perpendicular to the dimension of flow. A circular flow domain has been created around the airfoil. This circular domain has been divided into two halves. Boundary of one half has been defined as inlet and the boundary of the other half represents the outlet. The flow moves from left to right with the free stream velocity. The problem setup is shown in figure 3-1.

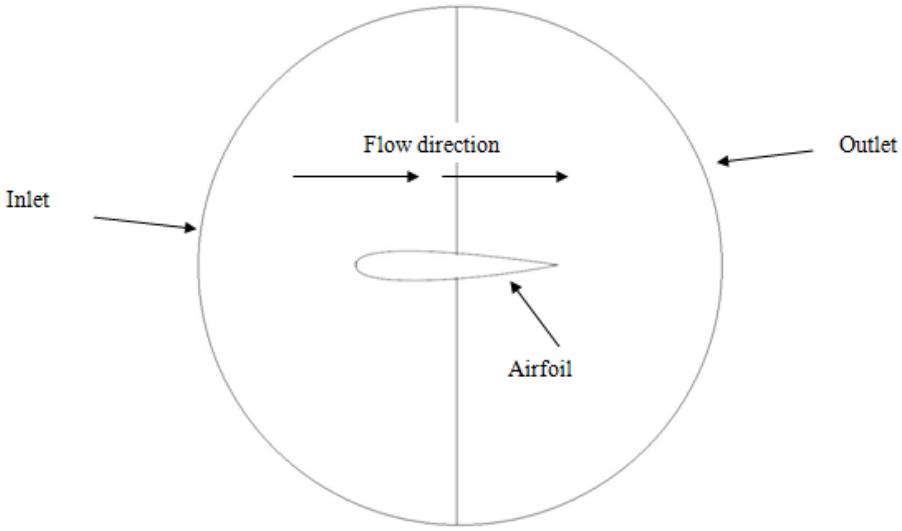

Figure 3-1 Schematic diagram of flow field around an airfoil

Zhao and Yang [16] employed NACA0014 for plunging motion. Therefore, NACA0014 has been chosen as baseline for the present research. It has been modeled in GAMBIT software by importing coordinates in the form of .txt file and exported to commercial CFD package software FLUENT for numerical computations. National Advisory Committee of Aeronautics (NACA) has designed airfoil shapes called NACA airfoils for aircraft wings. NACA airfoils are represented by four digits following the word NACA.

These four digits represent the profile of the airfoil. First digit represents the maximum camber of the airfoil as percentage of chord length. The distance of maximum camber from the leading edge of the airfoil in tens of percent of chord is represented by the second digit whereas the last two digits denote the maximum airfoil thickness in terms of percentage of chord length [23]. For NACA0014, 00 represents no camber and 14 describe the 14% thickness to chord length ratio. Profile of NACA0014 is shown in figure 3-2.

Figure 3-2 NACA0014 Profile

3.2 AIRFOIL MOTION KINEMATICS

Following equation defines the pure plunging motion of an airfoil

$$y(t) = hc\ Cos\ (\omega t) \qquad (3.1)\ [16]$$

where *y(t)* stands for instantaneous position of the airfoil, *h* denotes dimensionless stroke amplitude with respect to chord length, *c* represents the chord length of an airfoil section and ω is the angular frequency. Figure 3-3 represents the plunging motion of the airfoil.

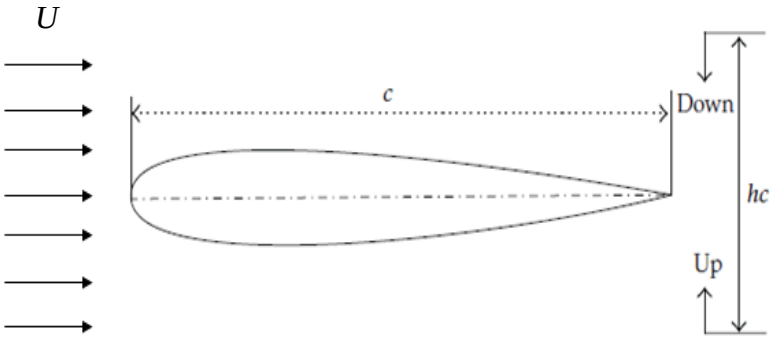

Figure 3-3 Plunging motion of an airfoil section [16]

3.3 NUMERICAL METHOD

Two dimensional unsteady Navier Stokes equations have been solved by using commercial CFD package based on finite volume technique. Details of conditions set in Fluent are as follows.

3.3.1 PRESSURE BASED SOLVER

Fluent uses two types of solvers

- Pressure based solver
- Density based solver

Pressure based solver is recommended for low speed incompressible flows whereas density based solver for high speed compressible flows. Velocity field is obtained from the momentum equations in both the methods. In pressure based solver, the pressure field is extracted by solving pressure or pressure correction equation which is obtained by manipulating continuity and momentum equations. In both methods fluent solves the governing integral equations for mass and momentum and for energy (when appropriate) and other scalars such as turbulence. Fluent uses finite volume technique in which domain is descretized into control volumes using computational grid. Governing equations are then integrated over individual control volumes to construct algebraic equations for unknowns (discrete dependent variables) variables such as velocity, pressure, temperature etc. Algebraic equations are then linearized and the resultant linear equations are solved to get updated values of unknown variables. Pressure-velocity coupling scheme has been used for the pressure based solver. In this scheme, pressure and velocity equations are solved in a fully coupled manner [24]. Flow chart of coupled pressure based solver is shown in figure 3-4.

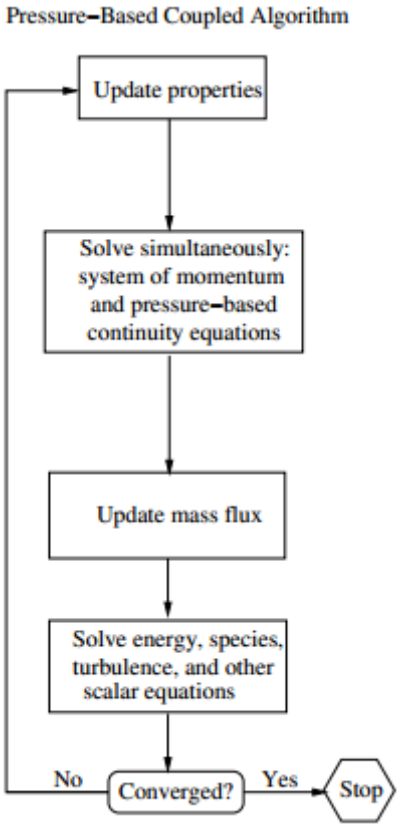

Figure 3-4 Flow chart of coupled pressure based solver [24]

Coupled pressure based solver offers five algorithms. PISO (Pressure implicit with splitting of operators) has been used for the present simulations. This algorithm is recommended for transient problems and it maintains a stable calculation with larger time step. So in order to save the computational time, this scheme has been chosen in the present research.

3.3.2 MESH

The descretization of a geometric domain into simple small elements is called mesh. There are generally two types of mesh, structured and unstructured mesh. In structured mesh, the word structured usually refers to the way the grid information is addressed by the computer [25]. In the structured mesh, a mapping function is constructed that transforms a curvilinear mesh to a uniform Cartesian grid. This allows a given's point neighbor to be easily identified and accessed which helps in speedy CFD calculations. Structured mesh is basically of three types that is C-grids, H-grids and O-grids. In this research, O-type mesh is made around the airfoil. An O-grid will have lines of points where the last point wraps

around and meets the first point as shown in figure 3-5. This will result in grid lines that look like the letter 'O'. [25, 26].

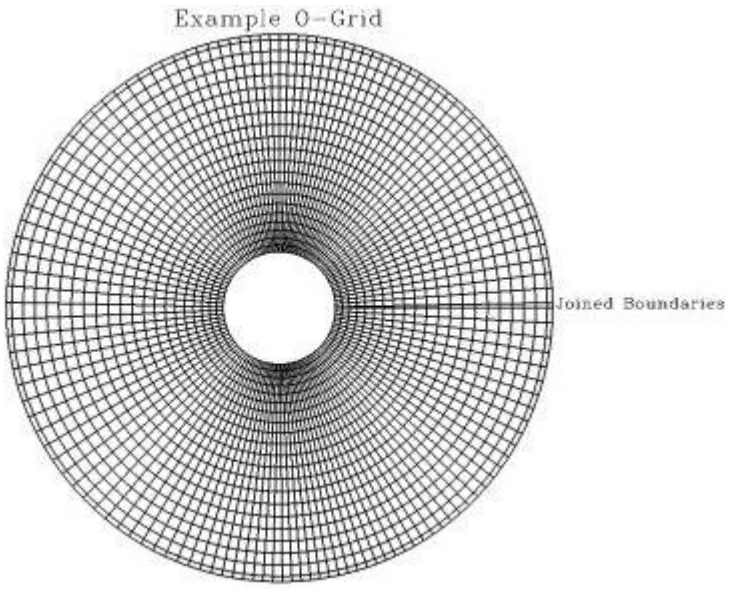

Figure 3-5 O-Type grid [25]

The purpose of using structured grid instead of unstructured grid is due to several reasons. Firstly, the structured grids run much faster than the unstructured grids. Although unstructured grids are much easier to create, a high quality structured mesh usually takes about as long as creating high quality unstructured mesh. Also the unstructured solvers are often (but not always) more dissipative as compared to a high resolution structured solver. Therefore unstructured grids are not unsuitable for some applications [25].

3.3.3 DESCRETIZATION

3.3.3.1 TEMPORAL DESCRETIZATION

Governing equations must be descretized in both space and time for transient simulations. In temporal descretization, every term in differential equation is integrated over time step Δt [24]. Integration of transient term is shown below

$$\frac{\partial \emptyset}{\partial t} = F(\emptyset) \qquad (3.2)\ [24]$$

where the function F represents any spatial discretization. First order accurate temporal descretization using backward differences is as follows

$$\frac{\emptyset^{n+1} - \emptyset^{n}}{\Delta t} = F(\emptyset) \qquad (3.3)\ [24]$$

The above equation has been solved implicitly as follows

$$\frac{\emptyset^{n+1} - \emptyset^{n}}{\Delta t} = F(\emptyset^{n+1}) \qquad (3.4)\ [24]$$

Above equation is implicit because $\emptyset^{n+1}$ in a given cell is related to $\emptyset^{n+1}$ in neighboring cell through $F(\emptyset^{n+1})$.

$$\emptyset^{n+1} = \emptyset^{n} + \Delta t\, F(\emptyset^{n+1}) \qquad (3.5)\ [24]$$

The implicit equation is solved iteratively at each time step before moving to the next time step. The advantage of using implicit scheme is that it is unconditionally stable with respect to time step size. In this study, initially two values of time steps have been used that is 1e-5 and 3e-5 for the validation studies. After performing validation studies, the time step size of 1e-5 has been finalized and used for further numerical simulations.

3.3.3.2 SPATIAL DESCRETIZATION

Fluent store the value of scalar Ø at all cell centers by default. Whereas the face values $Ø_f$ are required for convection terms. These values must be interpolated from the cell center values. This is achieved using an upwind scheme. In an upwind scheme the face value

$Ø_f$ is derived from the quantities in the upstream cell. Fluent offers several upwind schemes which includes first order upwind, second order upwind, power law and QUICK.

In pressure based solver, all the equations are solved by using first order upwind scheme for convection by default. When the flow is aligned with grid, first order upwind descretization can be used. This type of descretization scheme is used when the flow is aligned with the grid. For the flows which are not aligned with the grid, first order upwind descretization increases the numerical error. So for tetrahedral and triangular grids where the flow is not aligned with the grid, accurate results will be obtained by using the second order descretization. It also gives better results for quad/hex grids especially for complex flows. For rotating and swirling flows, the QUICK and third order MUSCL (Monotone Upstream-Centered Schemes for Conservation Laws) descretization are used because they give better convergence than the second order upwind descretiazation for these types of flows. In the present study, the second order upwind spatial descretization has been used because the airfoil is in plunge motion and due to complexity of flow [24].

3.3.4 BOUNDARY CONDITIONS

Flow variables specified at boundaries of computational model are known as boundary conditions. In present research simulations have been carried out at low Reynolds number that is 10,000 initially for the validation case. Boundary conditions on the outer surface of the computational domain are specified as inlet and outlet. Far field boundary conditions are therefore set as velocity inlet and pressure outlet. In velocity inlet boundary conditions, the flow velocity along with the scalar properties of the flow at the velocity is specified at the inlet. This type of boundary condition is used for incompressible flows. For compressible flows, setting velocity inlet boundary condition leads to nonphysical results. In the Pressure outlet boundary conditions, static (guage) pressure is specified at the outlet boundary. Free stream velocity is specified at inlet which is 34.7 m/sec in the present research whereas zero static pressure is defined at pressure outlet. A no-slip boundary condition is specified on the

wall of the airfoil surface which means that the incoming fluid will stick to the wall and moves with the same velocity as the wall, if it is moving. A reference pressure of 1 atm has been taken throughout the simulations.

3.3.5 TURBULENCE MODEL

Reynolds number is the parameter that characterizes the type of flow. It determines whether the flow is laminar or turbulent. At low Reynolds number, flow is usually assumed to be laminar. Flows at Reynolds number larger than 5000 are typically (but not necessarily) turbulent. Transport quantities fluctuate in turbulent flows. These fluctuations are small in scale but of high frequency. Therefore, it is computationally expensive to solve these equations directly in practical engineering calculations. These small scale fluctuations can be removed by time averaging the instantaneous transport equations which results in giving a modified set of equations that are computationally less expensive to solve. These modified equations contain additional unknowns and hence turbulence models are needed to solve these unknowns in terms of known quantities.

In this research, computations have been performed at Reynolds number of 1000, 10,000 and 25,000 respectively. Therefore, flow has been assumed as laminar at Reynolds number of 1000 and Spalart-Allmaras turbulence model (SA) model has been used for 10,000 and 25,000.

Initially, the baseline airfoil NACA0014 has been simulated by assuming the flow to be turbulent at Reynolds number of 10,000 and simulations were carried out using S-A and K-ε turbulence models. Results obtained by using S-A turbulence model are found to be in agreement with the literature. Therefore S-A turbulence has been finalized for simulating flows at high Reynolds number of 10,000 and 25,000 respectively.

The Spalart-Allmaras model is a one equation model that solves the modeled transport equation for eddy viscosity. It is usually recommended for wall bounded flows in

aerospace applications and has been found to give good results for applications in which boundary layer is subjected to adverse pressure gradients.

3.3.6 y^+ VALUE

y^+ is the non dimensional distance from the wall to the first grid point. A very fine mesh is required to resolve turbulence eddies in the boundary layer. The purpose of setting the y^+ value is to ensure enough resolution of boundary layer profile to get accurate turbulence effects [24]. This dimensionless wall distance is defined by the following equation

$$y^+ = \frac{u*y}{\nu} \qquad (3.6)$$

where, u is the friction velocity at the nearest wall, y is the distance to the nearest wall and ν is the local kinematic viscosity of the fluid. For present research, the value of y^+ is set equal to 1 while using S-A turbulence model during the computations.

3.3.7 DYNAMIC MESHING

Dynamic Meshing technique available in fluent is used when the shape of domain changes with time due to motion on the domain boundaries. This technique can be used for both steady and unsteady problems. There are two types of motion in this technique prescribed motion (in which the linear and angular velocities can be specified at the centre of gravity of solid body with time) and unprescribed motion (in which the subsequent motion is determined based on the solution at the current time). Volume mesh is updated automatically by FLUENT [24].

In the present research the motion kinematics of airfoil is achieved using User Defined Function (UDFs) based on the centre of gravity of airfoil. For defining the plunging motion of airfoil, DEFINE_CG_MOTION macro was used. It is then hooked in fluent in order to achieve the desired motion. Airfoil has been treated as rigid body and the whole mesh moves with the airfoil. The compiled UDF provides Fluent with the necessary angular

velocities at every time step and updates the node positions on dynamic zones based on solid body kinematics. UDF written in C language for plunging motion is given in Appendix-A.

Chapter 4: VALIDATIONS AND SENSTIVITY STUDIES

4.1 INTRODUCTION

This chapter focuses on the validation studies performed in order to assess the independence of numerical solver on grid and domain size. Time step sensitivity and turbulence model sensitivity studies has also been carried out to have the appropriate time step size and the turbulence model that may be able to capture the results.

4.2 FORCE CALCULATION

The aerodynamic performance of the plunging airfoil can be evaluated by computing lift coefficient (C_L) and drag coefficient (C_D) which can be calculated by the following equations

$$C_L = \frac{F_y}{0.5\rho U^2 S} \tag{4.1}$$

$$C_T = -C_D = \frac{F_x}{0.5\rho U^2 S} \tag{4.2}$$

where F_x and F_y represents the components of resulting aerodynamic force along the horizontal and vertical direction of airfoil surface, U is the free stream velocity, ρ is the density of the fluid and S is the reference area of airfoil which is equal to chord length (c) of an airfoil in 2D simulations. Therefore the time averaged lift and thrust coefficient can be evaluated from the following equation

$$C_T = -C_D = -\frac{1}{T}\int_t^{t+T} C_d\,(t)dt \tag{4.3}$$

$$C_L = \frac{1}{T}\int_t^{t+T} C_l\,(t)dt \tag{4.4}$$

4.3 GRID GENERATION

Grids for all the cases in this study has been generated using Gambit software and have same mesh topology that is O-type mesh as shown in figure 4-1. The grid lines normal to the airfoil surface and extending towards the outer surface are named as 'i' and the grid lines longitudinal to the airfoil surface cutting the normal grid lines are termed as 'j'.

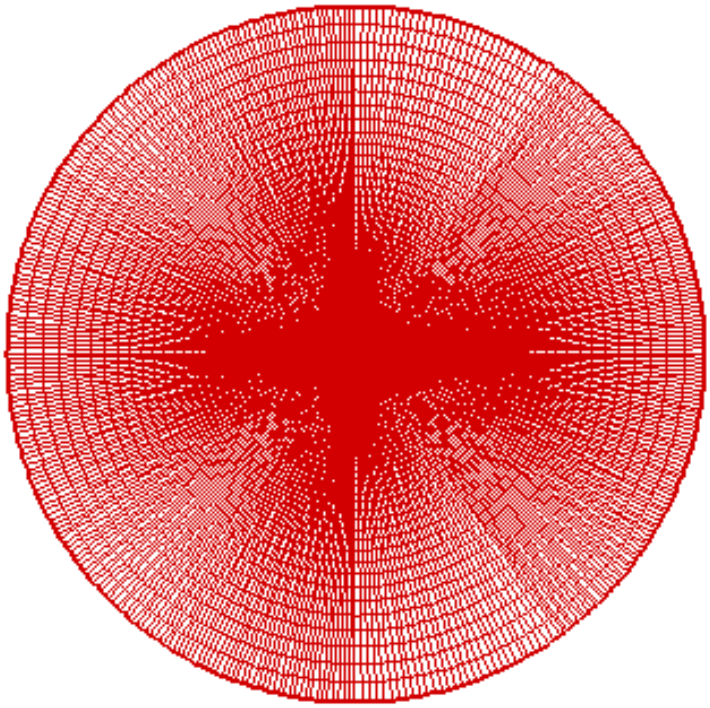

Figure 4-1 O – Type grid around the airfoil

The first grid point is located at a distance of 0.0002c through the edge meshing scheme of "First Length". This high density clustering near the airfoil ensures that $y+$ of approximately 1.0 is achieved for calculations involving turbulence models at higher Reynolds number and to provide a good computational space for the flow solution. Figure 4-2 shows the grid close up view.

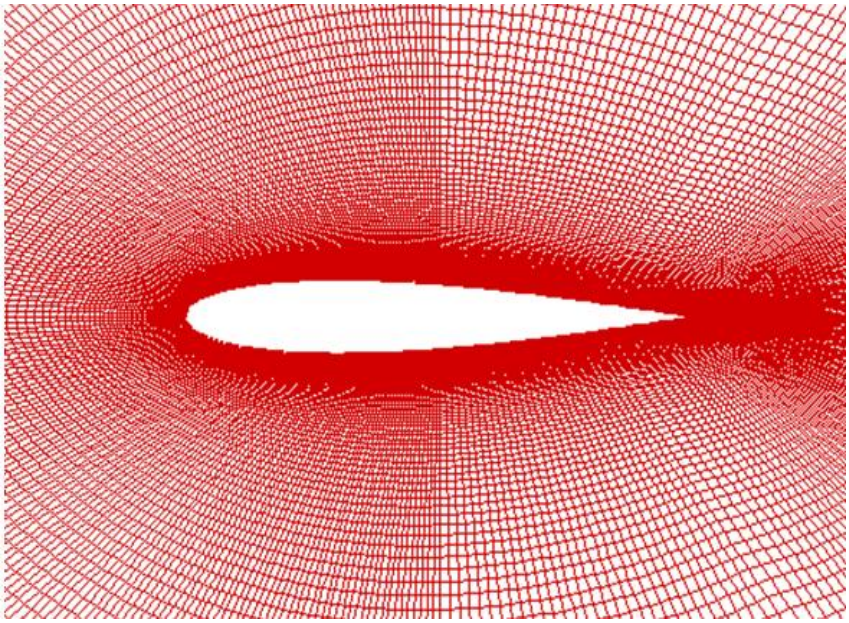

Figure 4-2 Grid close up view

4.4 VALIDATIONS AND SENSTIVITY STUDIES

Flow past plunging NACA0014 airfoil has been computed at Re = 10,000, h = 0.4, K = 2.0, U = 34.7 and c = 0.064 and compared to the published results of Liangyu Zhao and Shuxing Yang [16]. Following validations and sensitivity studies have been carried out in order to assess the independence of numerical solve over grid and domain and to choose appropriate time step size and turbulence model.

- Grid independence study
- Domain independence study
- Time step sensitivity study
- Turbulence model sensitivity study

4.4.1 GRID INDEPENDENCE STUDY

Grid independence study has been carried out to achieve a set of grid points for which the solution of the computational case does not further change if the grid points are increased in the computational domain. It has been performed by using two grid sizes that is 401×201(401 points on airfoil surface, 201 in vertical direction) and 401×301. Size of domain has been kept 20c with a time step size of 1e-5. Flow has been assumed as laminar

since the reference paper has simulated the plunging motion of the airfoil by assuming the flow to be laminar. Plots of lift and drag coefficients for both grid sizes are shown in figure 4-3 and 4-4 respectively. It is observe that plot of C_L is found to be in close agreement with the published results of Zhao and Yang [16] whereas the values of C_D are slightly over predicted which is due to the different grid topology and time step size used. Since the present is study is of qualitative nature and we are achieving 90-95% results, therefore these results are quite acceptable.

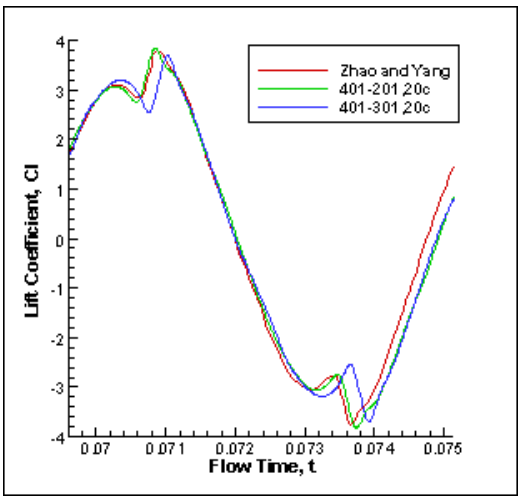

Figure 4-3 Time variation of lift Coefficient

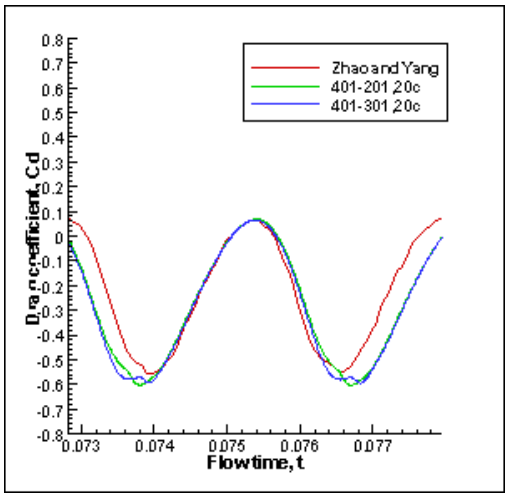

Figure 4-4 Time variation of drag Coefficient

4.4.2 DOMAIN INDEPENDENCE STUDY

The domains of 15*c* and 20*c* have been numerically solved for the grid dimension of 401 × 201. Grid size of 401×201 has been used with a time step size of 1e-5. Flow has been assumed as laminar. It is observed that even by changing domain sizes, there is no variation

in C_L and C_D plots as evident from figure 4-5 and 4-6 respectively. Results indicate the good agreement for both the domain extents. The values of drag are slightly over predicted in comparison with the values of published results. This may be due to the change of grid topology and time step size for the present study in comparison to the reference paper. As 90-95% of the results have been achieved, therefore the obtained results are acceptable and any one of the grid size can be used for further simulations.

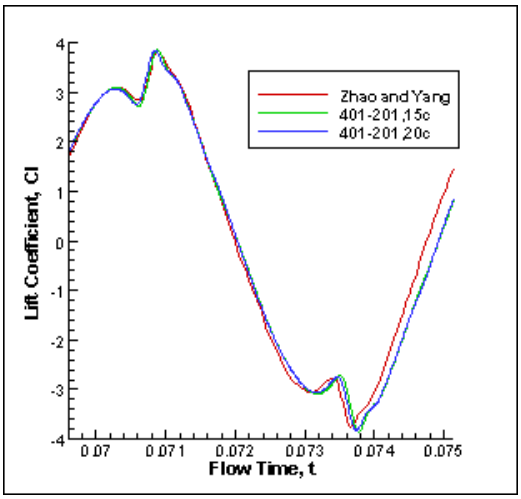

Figure 4-5 Time variation of lift Coefficient

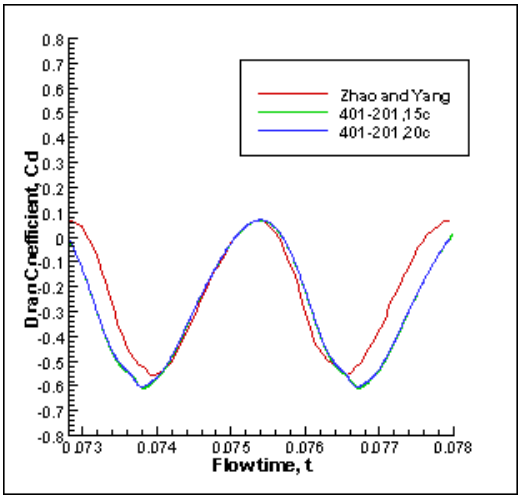

Figure 4-6 Time variation of drag Coefficient

4.4.3 TIME STEP SENSTIVITY STUDY

In time independent step sensitivity study, time step sizes of 1e-5 and 3e-5 has been used by keeping the domain size of 20c and grid size of 401×201. Laminar flow has been

assumed during the simulations.. Aerodynamic force coefficient plots obtained are shown in figure 4-7 and 4-8 respectively.

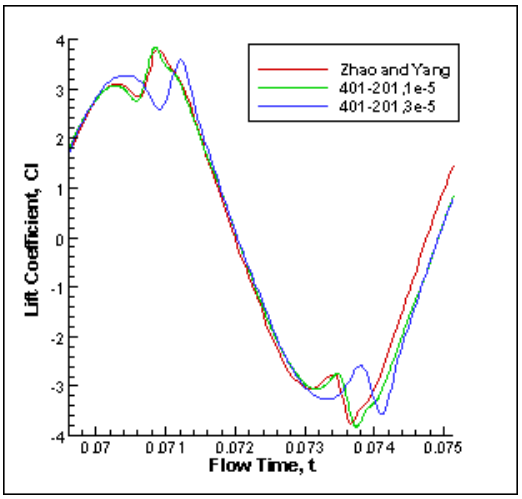

Figure 4-7 Time variation of lift Coefficient

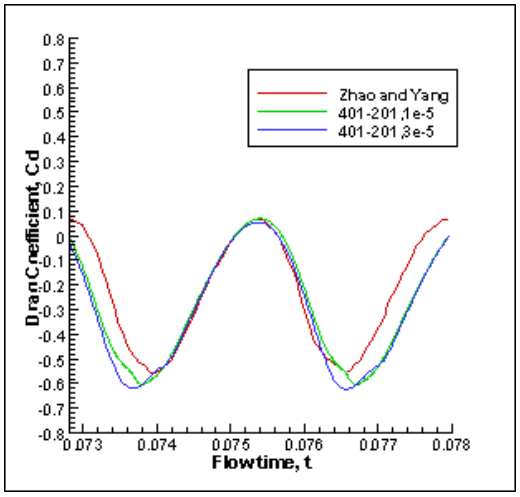

Figure 4-8 Time variation of drag Coefficient

Lift and drag plots obtained with the time step of 1e-5 are found to be in good agreement with the literature. The values of drag are over predicted with both the time step sizes. This may be due to the change of time step size used in the present study as compared to that used in the reference paper. So the same conclusion can be drawn as in the previous case that is the present study is of qualitative nature and 90-95 % of the results have been achieved. So the results obtained are quite acceptable.

4.4.4 TURBULENCE MODEL SENSTIVITY STUDY

In this research, simulations are also performed at both low and high values of Reynolds numbers. Therefore turbulence model sensitivity study has also been carried out in order to capture the turbulence effects at high Reynolds numbers of 10,000 and 25,000. For this purpose, S-A turbulence model and K-ε turbulence models has been used to simulate the plunging airfoil with the domain size of 20c, grid size of 401×201 and a time step of 1e-5.

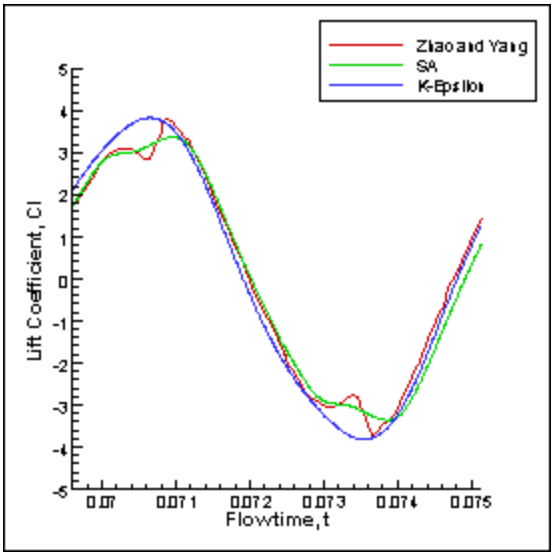

Figure 4-9 Time variation of lift Coefficient

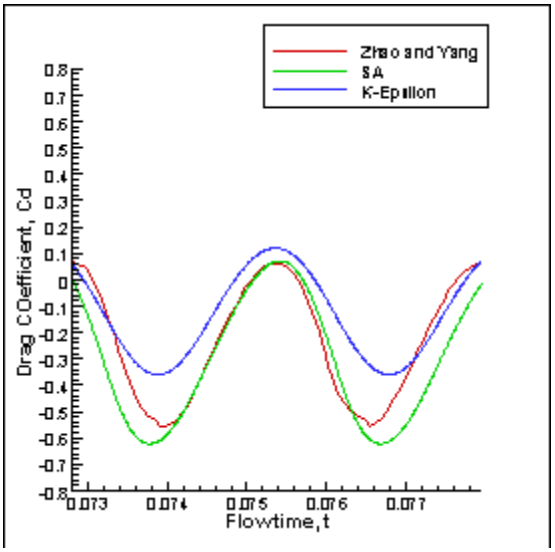

Figure 4-10 Time variation of drag Coefficient

Figure 4-9 and 4-10 represents the lift and drag time histories. It is seen that there is difference in the lift plots for the two cases as compared to original case. This difference is because the reference paper assumed the flow to be laminar, so the difference may be due to turbulence effects. Difference in the plots of drag histories is also observed. The value of drag is slightly over predicted with S-A turbulence model as compared to the reference paper which is again due to laminar flow assumption by Zhao and Yang [19]. Drag plot obtained with K- Ɛ turbulence model has a large difference in values with those of the reference case. It is because the value of y^+ of 1 has been maintained during the grid generation whereas different y^+ is recommended for K- Ɛ turbulence model.

4.5 CONCLUSION

From the above studies, it can be concluded that there is no change in the aerodynamic force coefficients even by changing domain and grid sizes. However, time step size of 1e-5 is giving better results as compared to 3e-5 which leads to the conclusion that higher time step size is unable to capture the flow physics. Based on these computations, domain size of 20c, grid size of 401×201, time step size of 1e-5 has been used for all the next simulations. For higher Reynolds number, SA model has been employed in order to capture turbulence.

Chapter 5: AIRFOIL SHAPE EFFECT ON AERODYNAMIC PERFORMANCE AND SYSTEMETIC INVESTIGATION OF REDUCED FREQUENCY AT REYNOLDS NUMBER (Re) OF 10,000

5.1 COMPARISON OF DIFFERENT SHAPES OF AIRFOILS ON AERODYNAMIC PERFORMANCE

This chapter covers the comparison of aerodynamic force coefficients of different shapes of airfoils in pure plunging motion at Reynolds number of 10,000. The cross sections used for comparison purpose include NACA0014, Ellipse and flat plate as shown in figure 5-1. Thickness of all the three cross sections of airfoils is kept constant that is 14% of chord length. Since the validation studies were performed on NACA0014, results of validation serve as baseline and lift and drag coefficients of the other two cross sections are compared with it. These cross sections has been chosen for comparison purpose as previous literature was focused mostly on these cross section airfoils for MAV applications but only independent studies that is the effect of various parameters which includes Reynolds number effect, reduced frequency effect, thickness effect etc were carried out.

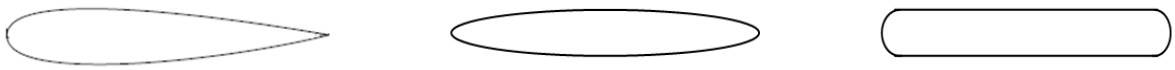

Figure 5-1 Cross sections of airfoils

C_L Vs time plot and C_D Vs time plot are shown in figure 5-2 and 5-3 respectively. These plots reveal that the variation of both C_L and C_D is sinusoidal in behavior. It is observed that C_L attains a maximum and minimum value of approximately +3.5 and -3.5 for all the three shapes of airfoils.

From C_D Vs time plot, the maximum value of C_D for ellipse is 0.1 and minimum value of C_D is -0.31. Similarly for flat plate, maximum and minimum value of C_D equals to

0.24 and -0.3. NACA0014 has C_D variation between 0.08 to -0.61. These values are shown in table 5-1.

Table 5-1 Instantaneous maximum and minimum values of coefficient of lift and drag at Re = 10,000, K = 2.0

Airfoil	Re = 10,000, K=2.0			
	$C_{L\,max}$	$C_{L\,min}$	$C_{D\,max}$	$C_{D\,min}$
NACA0014	+3.5	-3.5	0.08	-0.61
Ellipse	+3.5	-3.5	0.1	-0.31
Flat Plate	+3.5	-3.5	0.24	-0.3

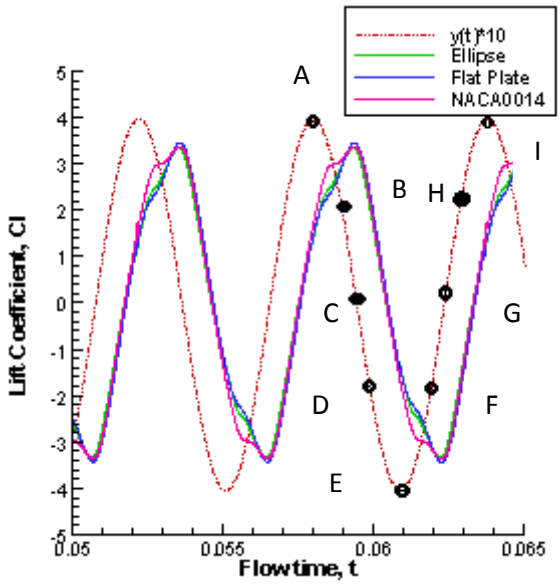

Figure 5-2 Lift Vs Time Plot, K = 2.0

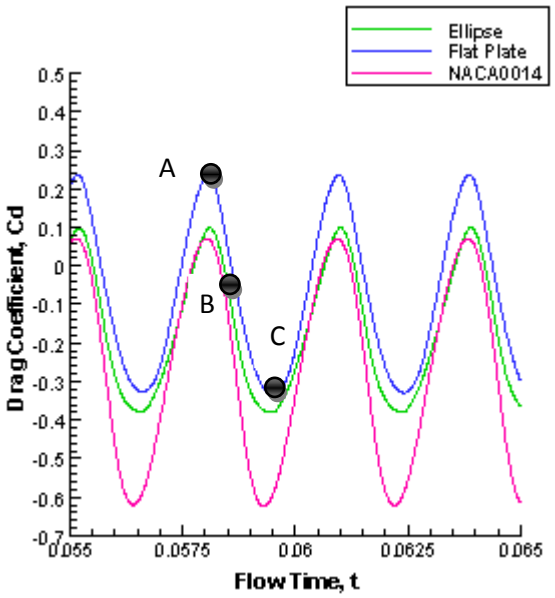

Figure 5-3 Drag Vs time Plot, K = 2.0

Figure 5-2 shows that lift Vs time plots for all the three cases are identical qualitatively as well as quantitatively. It is interesting to note that C_L attains a very high positive and negative values (cyclic symmetric in nature). However, there is a visible difference in C_D Vs time plots as shown in figure 5-3. Drag plots are quite similar in behavior but differ in values as evident from the graph. Ellipse and NACA0014 are more negative as compared to the flat plate. Now, this is a very interesting phenomenon that all the three shapes of airfoils are producing same

amount of lift but different amount of drag. In order to investigate the reason behind this phenomenon, flow physics of all the cases should be explored. For this purpose vorticity contours have been plotted for all the three cross sections of airfoils. But before comparing the flow physics of all the three cases, we will investigate why C_L attains very high positive and negative values as compared to drag. Therefore, considering the vorticity plots of a particular case that is NACA0014 as shown in figure 5-4. Vorticity contours have been plotted for eight points marked on displacement plot (y (t)) for one complete plunge cycle as shown in figure 5-2. These points are marked alphabetically from A to H. Figure 5-3 elaborates the position of the airfoil at these instants.

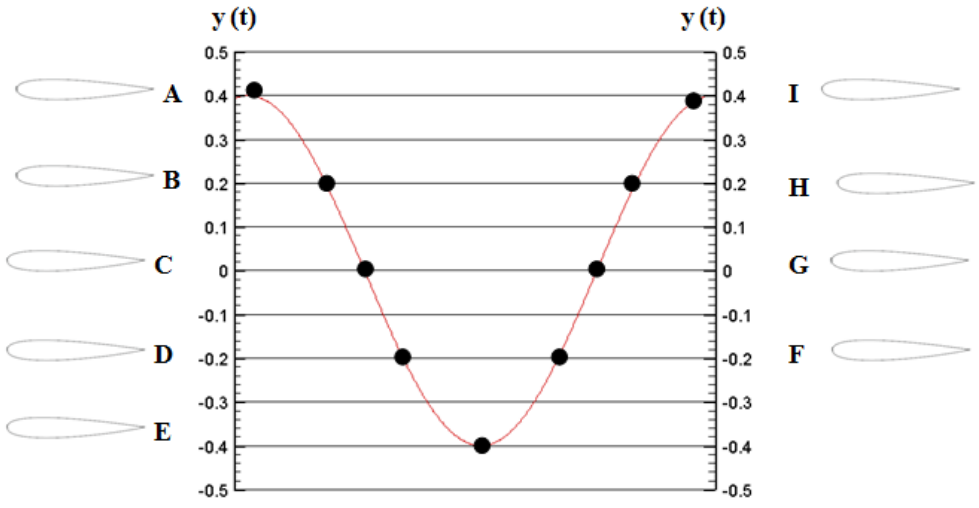

Figure 5-4 Position of the airfoil during one plunge cycle

Point A is the start of down stroke and the airfoil is at uppermost position. At this position low pressure vortex is located at the forward portion of lower side of the airfoil. At this point airfoil experiences positive lift because the local static pressure on the upper surface of airfoil is less than lower surface. From point A to C airfoil moves toward the midpoint of down stroke cycle and a new vortex is formed near the leading edge of airfoil while the vortex on the lower surface of the airfoil moves towards the trailing edge. At this point, airfoil experiences very high lift and value of coefficient of lift is maximum. From point C to E,

airfoil moves towards its lowest position which results in decreasing lift coefficient due to shedding of vortex from the trailing edge of the airfoil. Meanwhile, the vortex on upper surface of the airfoil moves towards centre along the chord of airfoil and lifts off the airfoil.

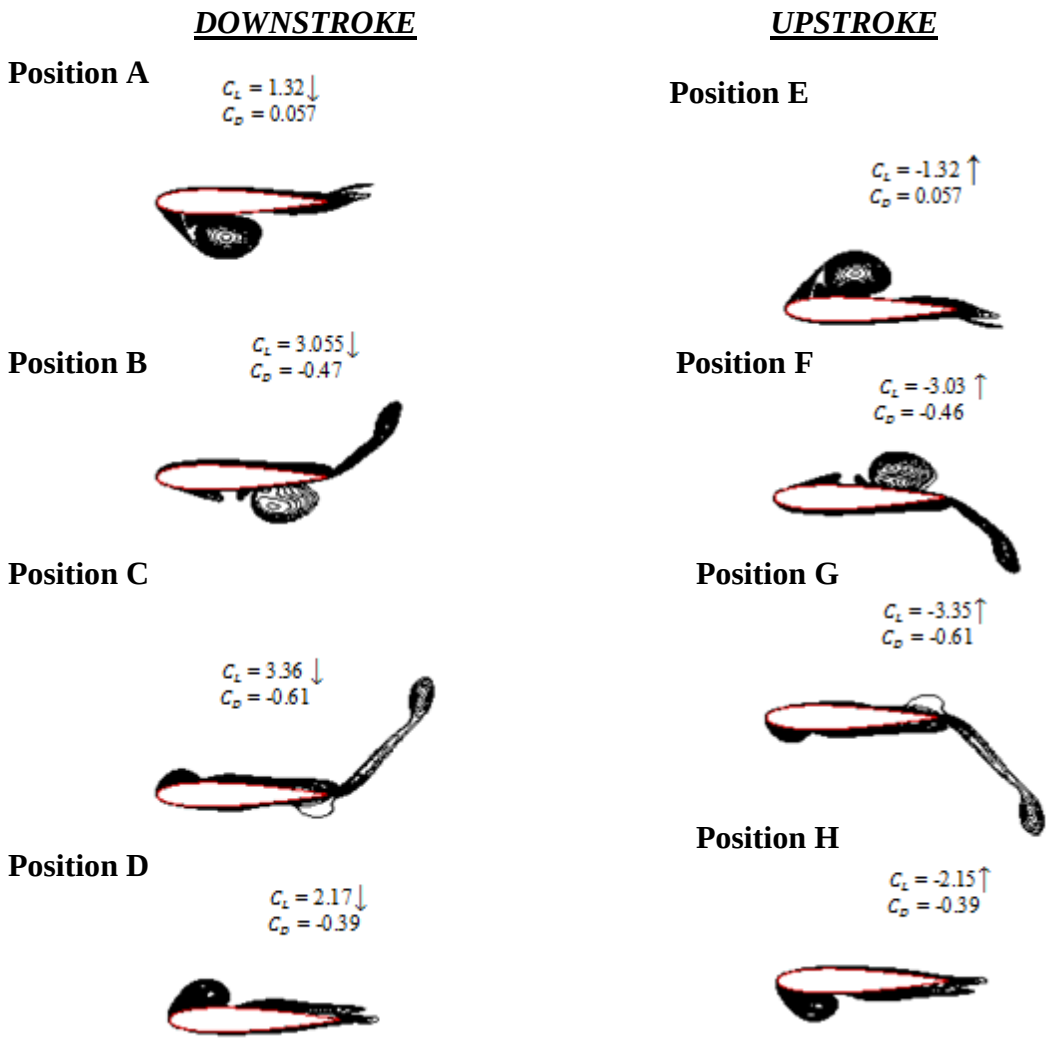

Figure 5-5 Vorticity contours of NACA0014

This leading edge separation and formation of vortex core shows that the forces acting on an airfoil are dominant by pressure and viscous forces are very small. Therefore, large pressure forces when multiplied by the value of Δx (which remains almost same for each element) gives very large positive and negative values of C_L.

NACA0014	ELLIPSE	FLAT PLATE
Position A		
$C_L = 1.32 \downarrow$ $C_D = 0.057$	$C_L = 1.07 \downarrow$ $C_D = 0.054$	$C_L = 1.09 \downarrow$ $C_D = 0.20$
		
Position B		
$C_L = 3.055 \downarrow$ $C_D = -0.47$	$C_L = 2.87 \downarrow$ $C_D = -0.28$	$C_L = 2.82 \downarrow$ $C_D = -0.18$
		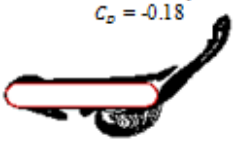
Position C		
$C_L = 3.36 \downarrow$ $C_D = -0.61$	$C_L = 3.33 \downarrow$ $C_D = -0.37$	$C_L = 3.44 \downarrow$ $C_D = -0.32$
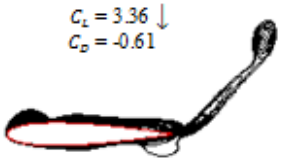		
Position D		
$C_L = 2.17 \downarrow$ $C_D = -0.39$	$C_L = 2.04 \downarrow$ $C_D = -0.30$	$C_L = 2.35 \downarrow$ $C_D = -0.26$
		
Position E		
$C_L = -1.32 \uparrow$ $C_D = 0.057$	$C_L = -1.07 \uparrow$ $C_D = 0.054$	$C_L = -1.08 \uparrow$ $C_D = 0.20$
		
Position F		
$C_L = -3.03 \uparrow$ $C_D = -0.46$	$C_L = -2.86 \uparrow$ $C_D = -0.28$	$C_L = -2.8 \uparrow$ $C_D = -0.17$
		

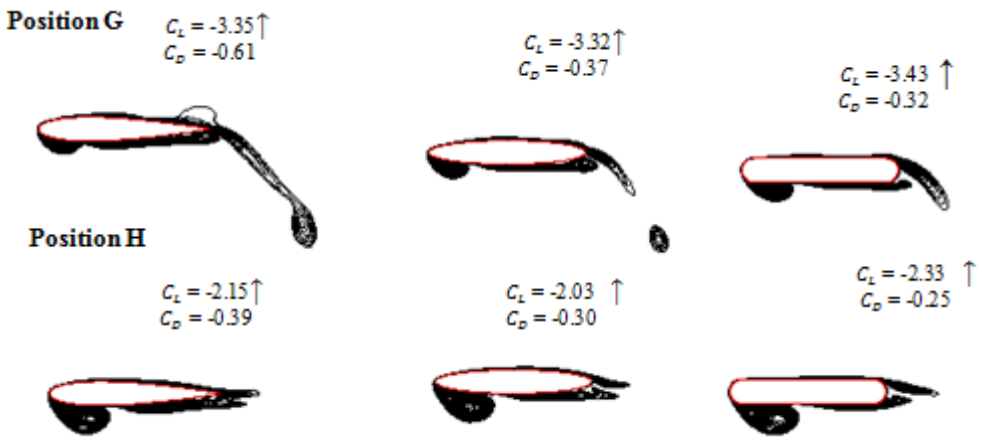

Figure 5-6 Vorticity plots of NACA0014, Ellipse and Flat Plate

Now comparing the vorticity plots of all the three shapes of airfoils as shown in figure 5-6. It is observed that vortex structures are quite similar at all the instants showing that each cross section is producing same amount of lift. Now the question arises regarding difference in C_D Vs time. In order to explore the difference in drag produced by the airfoils, considering only the ellipse and flat plate. Both the airfoils are divided into four halves as shown in figure 5-7. Ellipse is divided vertically at the point of maximum thickness that is 50% of chord length. Similarly, the flat plate is also divided vertically at half of the chord length. Horizontally both the airfoils are divided at centre that is at the chord of the airfoil.

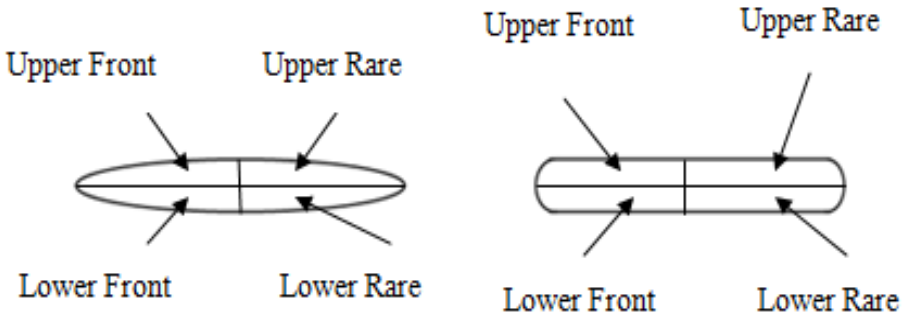

ELLIPSE **FLAT PLATE**

Figure 5-7 Four halves of ellipse and flat plate

The drag coefficient of the four halves of the airfoils is then found out by calculating the area under the curve of pressure coefficient Vs y at the three points representing the contribution of each half of the airfoil in the total drag at the particular point. These points are maximum, mean and minimum value of drag coefficient marked as point A, B and C in the figure 5-3. This represents the contribution of each half of the airfoil in the total drag at that point.

Figures 5-8, 5-9 and 5-10 represent the pressure coefficient plots of the two airfoils at point of maximum, mean and minimum values of drag coefficient and table 5-2 represents the values of coefficient of drag of four different halves of the airfoils at the three points. Also the Vorticity plots of both the airfoils at these three points are shown in figure 5-11, 5-12 and 5-13. For maximum value point, lower front portion of both the airfoils is producing maximum drag and the low pressure leading edge vortex almost reaches at the mid of the lower surface of the airfoils as evident from vorticity plots as this point (Figure 5-11). Hence this low pressure vortex starts to produce suction on the rare side of the airfoil which is also evident Cp Vs y plot at this point as shown in figure 5-8.

The pressure coefficient plot at mean value point shows that the elliptic airfoil is creating the large suction peak as compared to flat plate. The values of drag coefficient mentioned in table 5-2 also show that the upper front portion has negative drag coefficient which means that it is contributing in thrust. At this point the low pressure vortex reaches the lower rear portion of both the airfoils and contributes in drag production as the table 5-2 represents that the lower rear portions have maximum values of drag as compared to other halves. Hence at this point, upper front and lower rear portions are producing the major chunk of positive and negative drag by both the airfoils. At this point ellipse has more negative values as compared to flat plate.

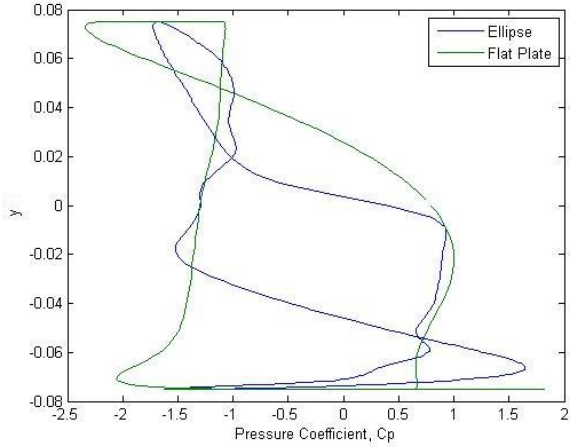

Figure 5-8 Cp Vs y plot at maximum value of drag coefficient

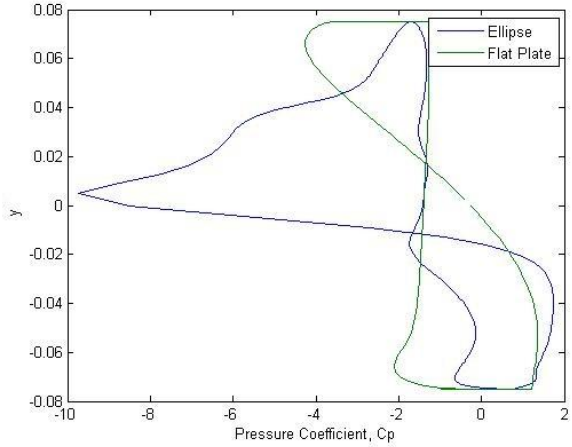

Figure 5-9 Cp Vs y plot at mean value of drag coefficient

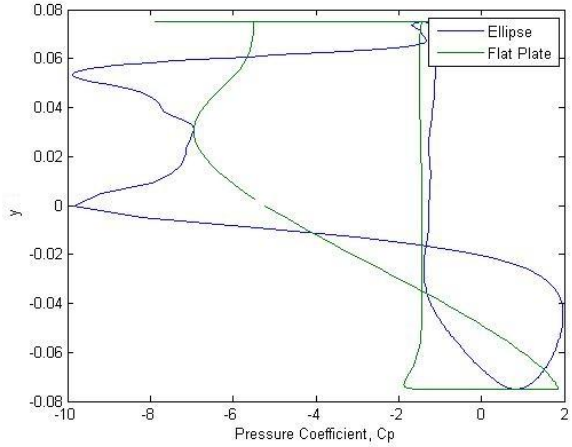

Figure 5-10 Cp Vs y plot at minimum value of drag coefficient

Figure 5-11 Vorticity plots at maximum value of drag coefficient

Figure 5-12 Vorticity plots at mean value of drag coefficient

Figure 5-13 Vorticity plots at minimum value of drag coefficient

Table 5-2 Drag coefficients of four halves of the airfoils

AIRFOIL HALVES	MAXIMUM POINT		MEAN POINT		MINIMUM POINT	
	Ellipse	**Flat Plate**	**Ellipse**	**Flat Plate**	**Ellipse**	**Flat Plate**
Upper front	0.0385	0.0795	-0.2489	-0.0650	-0.4072	-0.3835
Upper rear	-0.0414	-0.0431	-0.0232	-0.0339	-0.0162	0.0226
Lower front	0.1523	0.1848	-0.0183	0.1070	-0.0712	-0.1661
Lower rear	-0.0721	-0.0086	0.1121	0.0760	0.1292	0.1775
Coefficient of drag (Calculated)	**0.0773**	**0.2126**	**-0.1783**	**0.0841**	**-0.3654**	**-0.3455**
Coefficient of drag (From Cd plot at point c)	**0.09**	**0.234**	**-0.177**	**-0.1102**	**-0.380**	**-0.3329**

At the point of minimum value of drag, the pressure coefficient plot shows that ellipse is again showing the larger suction peak as compared to flat plate. Vorticity plots at this point show that low pressure leading vortex is formed at the upper front portion of both the airfoils which contributes in thrust production by lowering the values of drag coefficient this portion as shown in table 5-2. The value of ellipse is more negative as compared to flat plate as in the case of mean value point. The plots of Cp Vs y of mean and minimum value points shown in figure 5-9 and 5-10 represent that the leading edge of elliptic airfoil is creating the large suction peak. It is also observed that somewhere between y = 0 to y = 0.02 is actually taking the suction peak. In this region the leading edge curvature of ellipse is more prominent and produces less drag as compared to the flat plate. Therefore, we can say that the curvature has an effect on the thrust produced by the airfoil.

Drag acting on small element of the airfoil is given by the following expression

$$D = \int_A (-pdAsin\theta + \tau_\omega dAcos\theta) \qquad (5.1)$$

Where P represents the pressure forces that act normal to the surface of the airfoil whereas the τ_ω represents the shear forces acting tangential to the surface of the airfoil. So, the total drag acting on an object is due to the combined effects of pressure forces and wall shear. The part of the drag due to wall shear stress is called Skin friction drag since it is caused by frictional effects and the part due to pressure is called pressure drag. Pressure drag is also called form drag or profile drag. This type of drag generally arises due to the form or shape of the object whereas skin friction drag is caused due to the interaction of the particles of air to the surface of the airfoil. The expression in equation 5.1 shows that the pressure forces are multiplied by the $dAsin\theta$ which actually represents Δy (the height of element in vertical direction). Therefore, the integration of pressure and viscous forces around the airfoil (in x-direction) when multiplied by Δy (the height of element in vertical direction) results in change in magnitude of drag. For flat plate the value of Δy is prominent only at the leading

and trailing edges whereas for ellipse the value of Δy is there for most of the part of cross section. For NACA0014, Δy has greater value as compared to ellipse and flat plate and produces greater thrust.

Velocity vectors for the three airfoils have also been plotted at the same three points at which Cp plots have been drawn that is maximum, mean and minimum value of drag coefficients shown in figure 5-14. At the point of maximum values of drag coefficient, the low pressure region is at the middle of the lower surface of the airfoil. At the trailing edge, reversed flow is observed at the upper trailing edge. It is observed that the velocity vectors at this portion are in opposite direction to that of free stream direction. Moreover, significant difference is observed for the three airfoils at the trailing edge. For NACA0014 and ellipse more of the velocity vectors are in opposite direction to free stream direction showing that these vectors are contributing in thrust and hence lowers the value of coefficient of drag as compared to flat plate.

At the mean value point of drag coefficient, a low pressure region is found to separate from the leading edge of the three airfoils. More velocity vectors are observed to change their direction opposite to free stream in case NACA0014 as compared to ellipse. Therefore the more reverse flow is induced for NACA0014 and ellipse. For flat plate flow reversal is negligible and high value of drag coefficient at this point as compared to the other two airfoils.

For minimum value point, the low pressure region significantly increases for the three airfoils at the leading edge decreasing the value of coefficient of drag. Strong flow reversal is observed in case of NACA0014 as compared to ellipse as more of the velocity vectors are observed in the opposite direction of free stream and hence producing more thrust. However, for flat plate least flow reversal is observed as compared to other two airfoils.

NACA0014 **ELLIPSE** **FLAT PLATE**

Maximum point

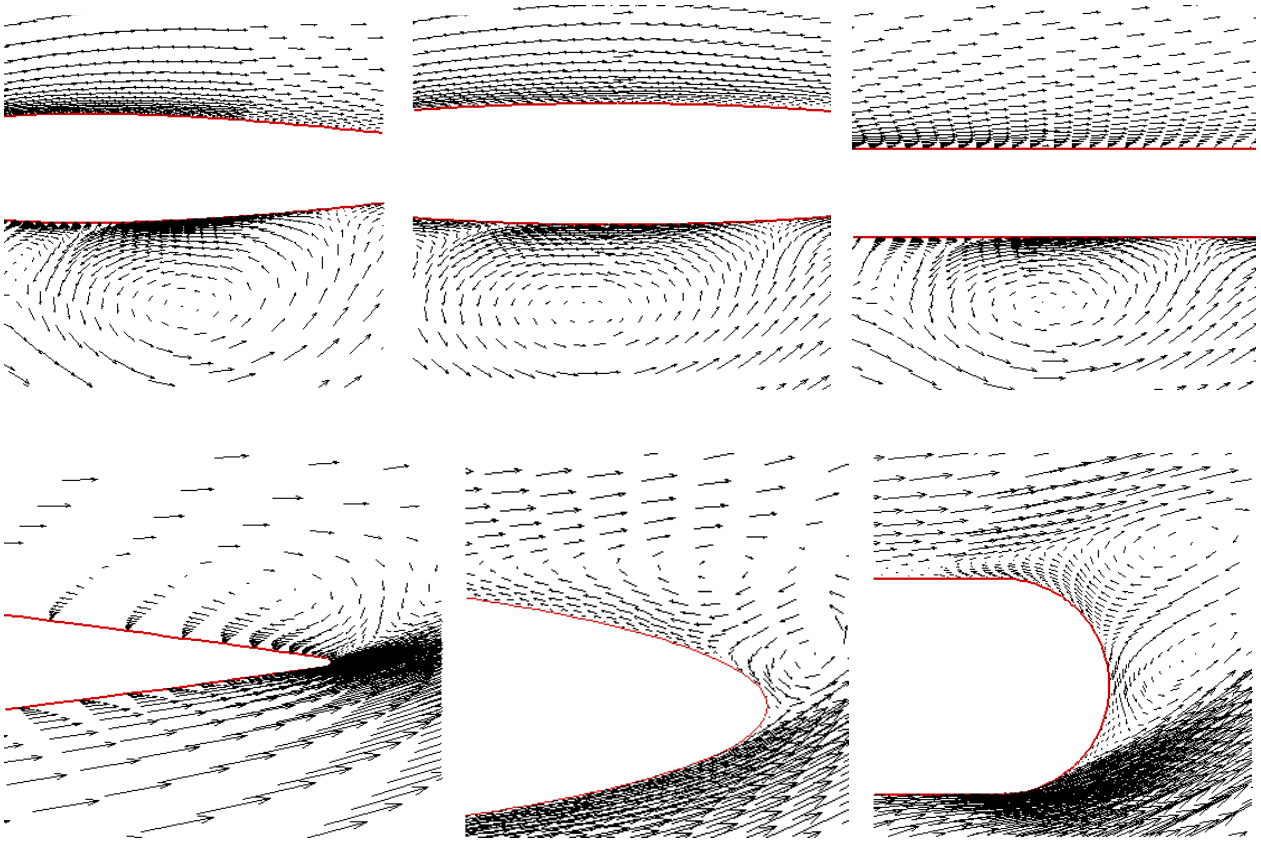

Mean point

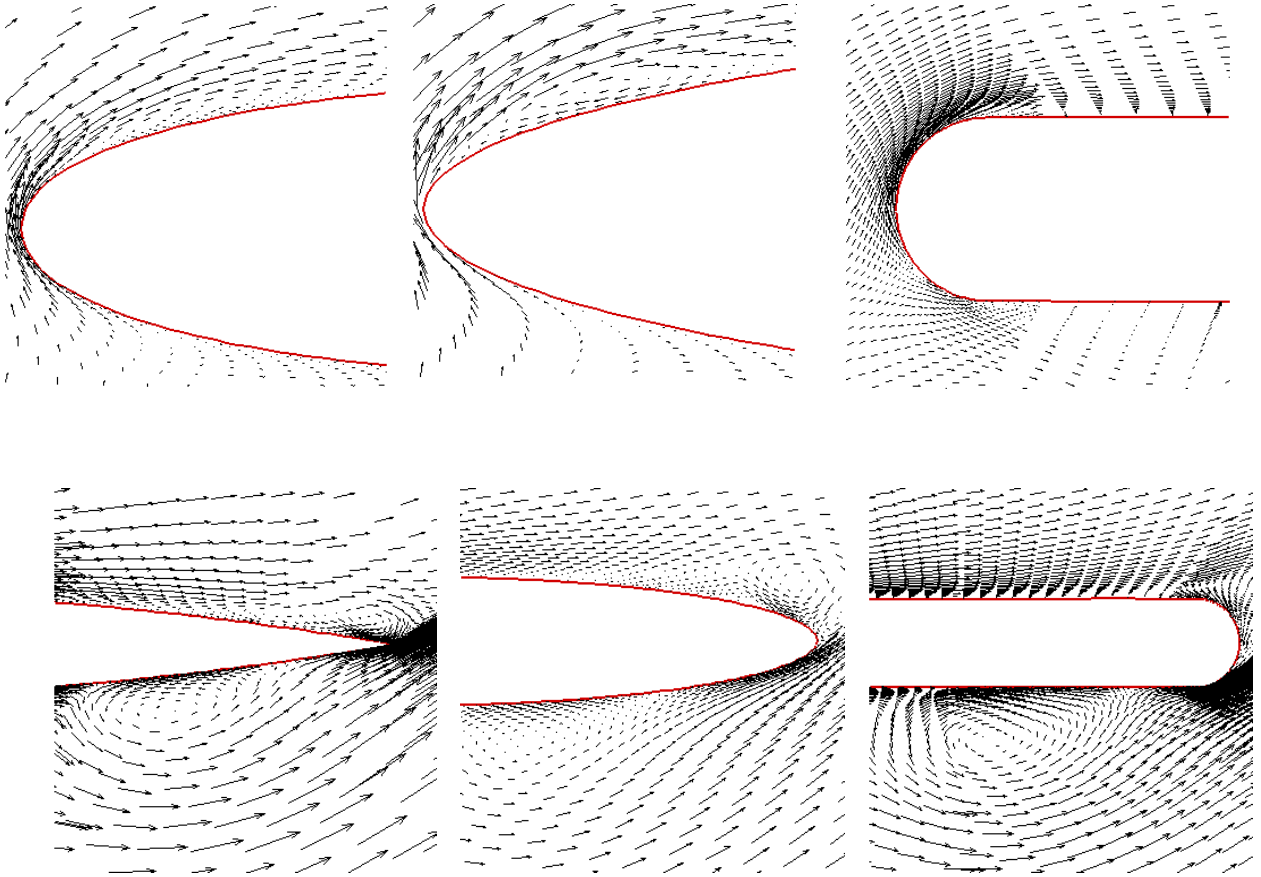

NACA0014 **ELLIPSE** **FLAT PLATE**

Minimum point

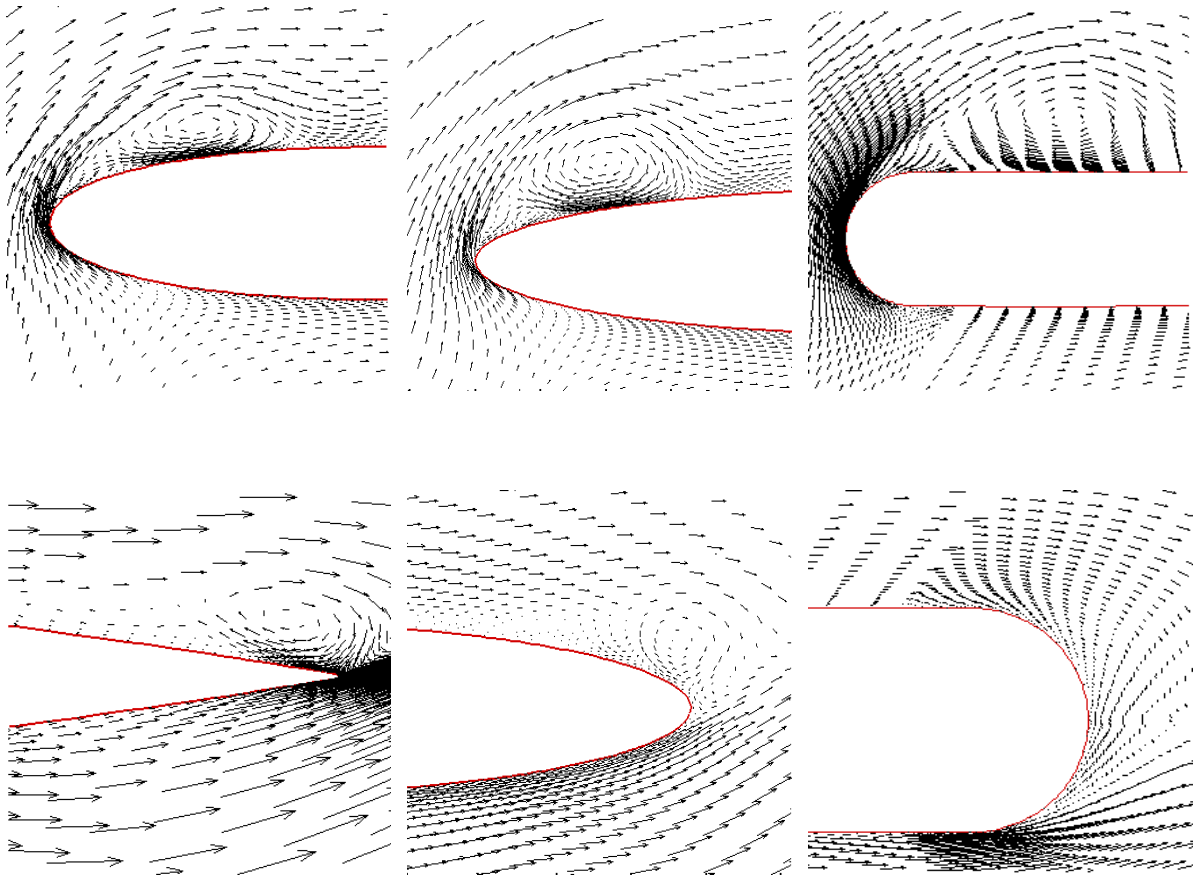

Figure 5-14 Velocity vectors of NACA0014, Ellipse and Flat Plate

Now investigating the contribution of viscous forces for the three airfoils. Table 5-3 represents the contribution of pressure and viscous forces of the three airfoils at the point of minimum value of drag coefficient. These values show that pressure forces are dominating. The value of viscous coefficient is negative for both NACA0014 and ellipse. These values of viscous coefficients show that the shear forces are thrust producing. Also the percentage contribution of viscous forces in thrust production is greater for NACA0014 (that is 2.5%) as compared to ellipse (only 1.3%). For flat plate, the value of viscous coefficient is positive which shows that viscous forces are drag producing in case of flat plate and their contribution is even greater than thrust producing viscous forces for NACA0014 and ellipse. These values of viscous coefficient

of the three airfoils justify the conclusions drawn by observing velocity vectors of the three airfoils

Table 5-3 Contribution of pressure and viscous forces at point of minimum value of drag coefficient

Airfoil	Re = 10,000, K = 2.0						
	Pressure force n	Viscous force n	Total force n	Pressure coefficient C_p	Viscous coefficient C_V	Total coefficient C_D	C_V/C_D
NACA0014	-28.65	-0.78	-29.43	-0.60	-0.016	-0.62	2.5%
Ellipse	-17.66	-0.25	-17.91	-0.37	-0.005	-0.37	1.3%
Flat Plate	-16.14	0.44	-15.70	-0.34	0.009	-0.33	2.7%

Table 5-4 represents the mean values of drag and lift coefficients of all the three cross sections. It is observed that time average lift coefficient over one complete cycle is zero whereas time averaged drag coefficient is nonzero. This is due to the fact that the cycle of motion of an airfoil is symmetric. Since lift vector acts perpendicular to the surface of airfoil, during down stroke it is pointed upward and during upstroke it acts in the downward direction. Both the vectors cancel each other and hence yield zero mean value.

Table 5-4 Mean Values of C_L and C_D

Airfoil	Re = 10,000, K=2.0	
	$\overline{C_L}$	$\overline{C_D}$
NACA0014	0.00	-0.27
Ellipse	0.00	-0.17
Flat Plate	0.00	-0.07

However, drag vector does not change its direction as it acts along the surface of the airfoil. During upstroke and down stroke, only the alignment of the drag vector is changed. Hence we find a finite value of drag. Also all the three crossections produce negative drag. As thrust

is negative of drag, hence thrust is produced by all the three shapes of airfoils. The reason behind the thrust generation instead of drag is due to the formation of Reverse Karman Vortex Shedding in the wake of airfoil in which the upper row consists of counter clockwise vortices and lower row consists of clockwise vortices as evident from figure 5-5. These vortices are momentum surplus as compared to the upstream flow and gives thrust to the airfoil.

5.2 REDUCED FREQUENCY EFFECT

Reduced frequency is actually the non dimensionalized form of flapping frequency It is used to describe the flapping frequency of the airfoil. Systematic investigation of reduced frequency has been carried out to see the effect on aerodynamic performance by seeing the flow behavior of the plunging airfoils. For this purpose, computations were also performed at reduced frequencies of K = 1.0 and K = 0.5 for same conditions as defined in the previous section for reduced frequency of K = 2.0. The corresponding values of the above mentioned reduced frequencies in Hz are shown in the table 5-5.

Table 5-5 Reduced frequencies and their corresponding values in Hz

REDUCED FREQUENCY *K*	**FLAPPING FREQUENCY (Hz)**
2.0	172.5
1.0	86.2
0.5	43.1

These values of flapping frequencies in Hz give the information about the flapping cycle of the plunging airfoil. For reduced frequency K = 2.0, the corresponding flapping frequency in hertz is 172 which shows that airfoil plunges 172 times per second. This means that the airfoil completes it flapping cycle that is wing up, wing down and wing up, 200 times every second. Similarly, K = 1.0 and 0.5 represents that the airfoil flaps 86 and 43 times per second. It is seen that with the decrease in value of reduced frequency, the value of flapping

frequency in Hz also decreases. This means that decreasing reduced frequency causes the number of flaps to reduce and hence the unsteady effect is also reduced. As for biological flyers, the flapping frequency ranges between 10-600 Hz [27], the chosen frequencies are within this range showing that the choice of reduced frequencies is suitable for present study.

Figure 5-15 and 5-16 show the C_L Vs time and C_D Vs time plots at reduced frequency, of K = 1.0 and figure 5-17 and 5-18represent the lift and drag time histories at reduced frequency of K = 0.5 respectively.

Lift Vs time plot for reduced frequency K = 1.0 shows that maximum and minimum values of coefficient of lift for NACA0014 and ellipse are almost equal that is 1.5 and -1.4 respectively. Flat plate has a slightly higher value of coefficient of lift that is 1.7 and -1.7.

From drag history, flat plate has a maximum and minimum value of C_D equal to 0.11 to -0.79 respectively. Ellipse has C_D variation between 0.08 to -0.16 and NACA0014 has 0.06 to -0.21. These values of maximum and minimum lift and drag coefficients are given in table 5-6.

Similarly for K = 0.5, the value of coefficient of lift has been reduced as evident from figure 5-17. For ellipse C_L varies between 0.65 and -0.65. NACA0014 has C_L variation between 0.7 and -0.7 whereas for flat plate lift coefficient has maximum and minimum value of 1 and -1 as shown in table 5-7.

From figure 5-18, value of C_D varies between 0.076 and 0.025 for flat plate, 0.05 and -0.03 for ellipse and 0.04 to -0.05 for NACA0014 as presented in table 5-7.

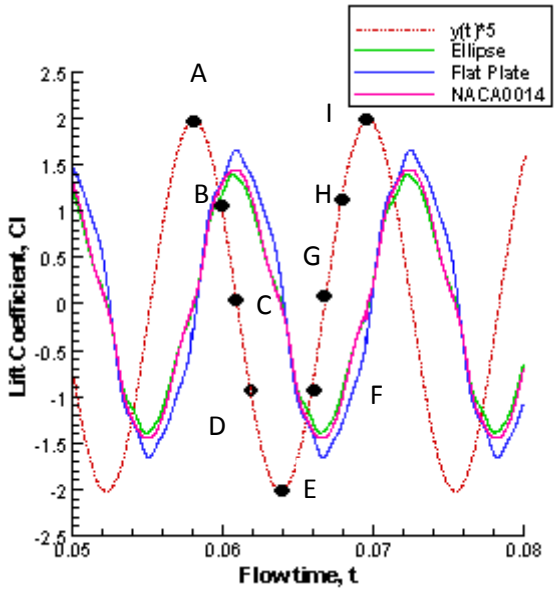

Figure 5-15 Lift Vs Time Plot, *K* = 1.0

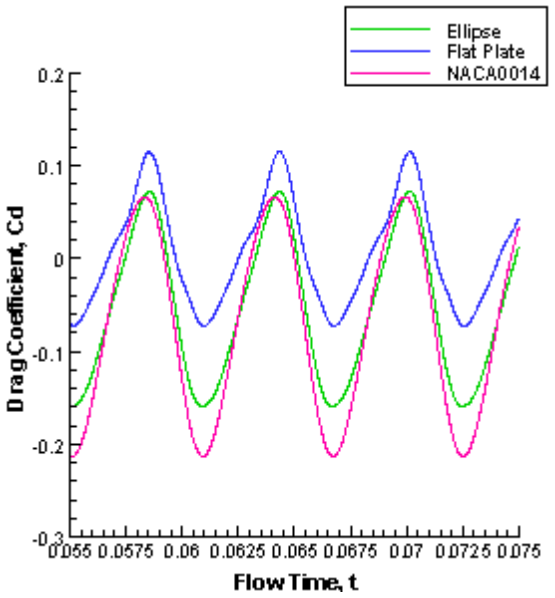

Figure 5-16 Drag Vs time Plot, *K* = 1.0

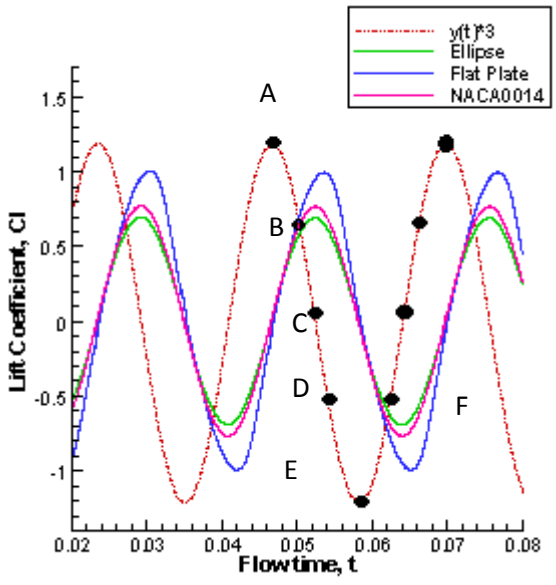

Figure 5-17 Lift Vs Time Plot, *K* = 0.5

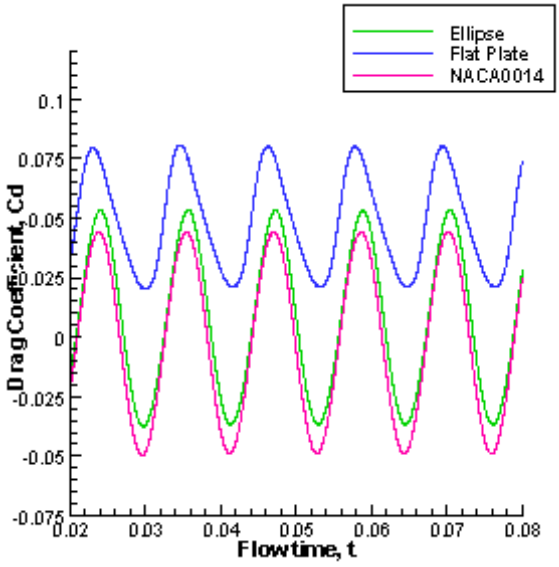

Figure 5-18 Drag Vs time Plot, *K* = 0.5

Table 5-6 Instantaneous maximum and minimum values of coefficient of lift and drag at Re = 10,000, K=1.0

Airfoil	Re = 10,000, K = 1.0			
	$C_{L\,max}$	$C_{L\,min}$	$C_{D\,max}$	$C_{D\,min}$
NACA0014	+1.5	-1.4	0.06	-0.21
Ellipse	+1.5	-1.4	0.08	-0.16
Flat Plate	+1.7	-1.7	0.11	-0.79

Table 5-7 Instantaneous maximum and minimum values of coefficient of lift and drag at Re = 10,000, K= 0.5

Airfoil	Re = 10,000, K= 0.5			
	$C_{L\,max}$	$C_{L\,min}$	$C_{D\,max}$	$C_{D\,min}$
NACA0014	+0.7	-0.7	0.04	-0.05
Ellipse	+0.65	-0.65	0.05	-0.03
Flat Plate	+1.0	-1.0	0.076	0.025

From above discussion of instantaneous maximum and minimum values of C_L and C_D, we can conclude that the value of C_L decreases with the decrease in the value of reduced frequency. Also the maximum value of coefficient of lift becomes slightly greater for flat plate as compared to ellipse and NACA0014. However, the plots of coefficient of drag shifted towards the positive values with the decrease in the reduced frequency (K) indicating that the thrust produced by the airfoils is decreased. The value of coefficient of lift decreases because the vortex becomes the sizable fraction of chord before separating at reduced frequency K = 1.0 as evident from vorticity contours in figure 5-19. A very high value of coefficient of lift for flat plate is also observed as compared to other two cross sections which is due to the formation of stronger vortex as compared to NACA0014 and

ellipse as observed in figure 5-19. At K = 0.5, low pressure vortex is not formed in case of ellipse and NACA0014 because at such low reduced frequency unsteady effect is not very prominent whereas for flat plate low pressure vortex is visible which is responsible for high value of lift coefficient as compared to the other two cases.

Table 5-8 Mean lift and drag coefficients at K = 2.0, K = 1.0, K = 0.5, Re = 10,000

Airfoil	K = 2.0		K = 1.0		K = 0.5	
	$\overline{C_L}$	$\overline{C_D}$	$\overline{C_L}$	$\overline{C_D}$	$\overline{C_L}$	$\overline{C_D}$
NACA0014	0.00	-0.27	0.00	-0.067	0.00	-0.002
Ellipse	0.00	-0.17	0.00	-0.05	0.00	0.007
Flat Plate	0.00	-0.07	0.00	0.01	0.00	0.048

Table 5-8 represents the mean values of Coefficient of drag and lift at all reduced frequencies that is K = 2.0, 1.0 and 0.5 respectively. It is seen that at reduced frequency K = 2.0, thrust is produced by all the three shapes of airfoils. When the value of reduced frequency has been reduced to K = 1.0, value of mean coefficient of drag increases for all the three cases. Value of mean coefficient of drag remains negative for NACA0014 and ellipse for this reduced frequency showing that very small amount of thrust is produced at K = 1.0 whereas for flat plate $\overline{C_D}$ becomes positive showing no thrust generation. For K = 0.5, value of $\overline{C_D}$ becomes zero for NACA0014 and ellipse and greater than zero for flat plate. In order to explore the reason behind this reduction in thrust generation, vorticity contours of all the three cross sections have been plotted as shown in figure 5-19 and 5-20. It is observed that the vertical spacing between the two rows of vortices in the wake decreases with the decrease in reduced frequency which reduces the thrust produced the airfoil. Also the wake is found to be near the airfoil for K = 2.0 hence producing a significant amount of thrust. For K = 1.0, wake vorticity is located farther from the airfoil which results in reduction of thrust. Similarly, for K = 0.5, wake vorticity moves further away from airfoil which results in drag

production. Pressure and viscous forces at reduced frequencies of K = 1.0 and 0.5 are tabulated in table 5-9 and 5- 10 respectively. At reduced frequency of K = 1.0, although the unsteady effect is reduced the pressure forces are still dominating as visible difference is there for all the three cases. For K = 0.5, the values of pressure forces are very low and also the difference in values for the three shapes is not very prominent. Hence as the unsteady effect is reduced, the contribution of viscous forces in drag starts increasing and airfoil shape effect is reduced.

Table 5-9 Pressure and viscous forces for the three shapes of airfoils at Re =10,000 and K = 1.0

Airfoil	Re = 10,000, K=1.0					
	Pressure force n	Viscous force n	Total force n	Pressure coefficient	Viscous coefficient	Total coefficient
NACA0014	-10.15	0.09	-10.06	-0.21	0.001	-0.21
Ellipse	-7.76	0.23	-7.52	-0.16	0.004	-0.15
Flat Plate	-3.96	0.54	-3.42	-0.08	0.011	-0.07

Table 5-10 Pressure and viscous forces for the three shapes of airfoils at Re = 10,000 and K = 0.5

Airfoil	Re = 10,000, K = 0.5					
	Pressure force n	Viscous force n	Total force n	Pressure coefficient	Viscous coefficient	Total coefficient
NACA0014	-2.99	0.67	-2.31	-0.063	0.014	-0.049
Ellipse	-2.53	0.79	-1.73	-0.05	0.016	-0.036
Flat Plate	0.38	0.61	1.0	0.008	0.012	0.02

SUMMARY

From the above discussion, following points can be summarized

a) Variation of C_L and C_D is sinusoidal in behavior with respect to flow time.

b) All the airfoils produces same amount of lift at high reduced frequency of K=2.0 at the given Reynolds number whereas there is a visible difference in thrust produced by each shape of airfoil.

c) Vorticity plot of all the three cases are similar showing that same amount of lift is produced by each cross section.

d) Difference in thrust produced by the airfoils is due to change in geometry of airfoil showing that shape effect is dominant at high reduced frequencies and at high Reynolds number of 10,000.

e) At low reduced frequencies, flat plate produces high lift coefficient and the difference in thrust produced by the three shapes of airfoils starts to decrease.

NACA0014	ELLIPSE	FLAT PLATE

Position A

C_L = -0.069↓ C_D = 0.053	C_L = -0.12↓ C_D = 0.039	C_L = -0.44↓ C_D = 0.070
		

Position B

C_L = 1.27↓ C_D = -0.11	C_L = 1.15↓ C_D = -0.082	C_L = 1.29↓ C_D = -0.016
		

Position C

C_L = 1.44↓ C_D = -0.21	C_L = 1.38↓ C_D = -0.15	C_L = 1.65↓ C_D = -0.070
		

Position D

C_L = 1.21↓ C_D = -0.15	C_L = 1.12↓ C_D = -0.12	C_L = 1.41↓ C_D = -0.041
		

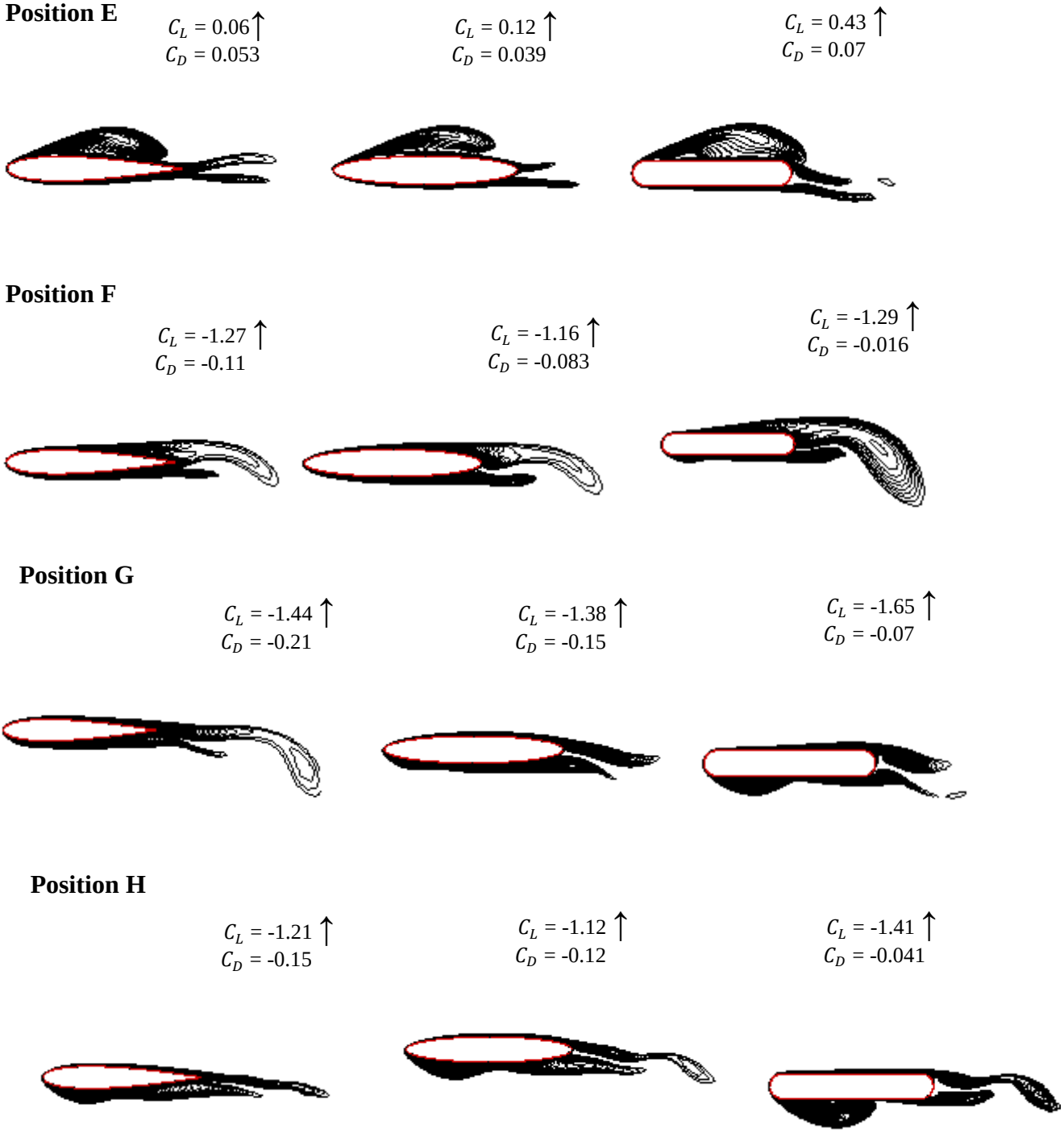

Figure 5-19 Vorticity Contours of NACA0014, Ellipse and Flat Plate at *K*=1.0

NACA0014	ELLIPSE	FLAT PLATE

Position A

C_L = 0.84↓ C_D = 0.041	C_L = 0.83 ↓ C_D = 0.047	C_L = 0.82↓ C_D = 0.08
		

Position B

C_L = 0.63 ↓ C_D = -0.01	C_L = 0.57↓ C_D = 0.00	C_L = 0.69↓ C_D = 0.04
		

Position C

C_L = 0.76 ↓ C_D = -0.04	C_L = 0.69↓ C_D = -0.03	C_L = 0.92↓ C_D = 0.02
		

Position D

C_L = 0.67 ↓ C_D = -0.03	C_L = 0.60↓ C_D = -0.02	C_L = 0.98↓ C_D = 0.02
		

NACA0014	ELLIPSE	FLAT PLATE

Position E

C_L = 0.17 ↑
C_D = 0.04

C_L = 0.18 ↑
C_D = 0.04

C_L = 0.27 ↑
C_D = 0.079

Position F

C_L = -0.63↑
C_D = -0.01

C_L = -0.57↑
C_D = 0.00

C_L = -0.69↑
C_D = 0.04

Position G

C_L = -0.76 ↑
C_D = -0.04

C_L = -0.69 ↑
C_D = - 0.03

C_L = -0.93 ↑
C_D = 0.024

Position H

C_L = -0.67 ↑
C_D = -0.03

C_L = -0.60 ↑
C_D = -0.02

C_L = -0.98 ↑
C_D = 0.024

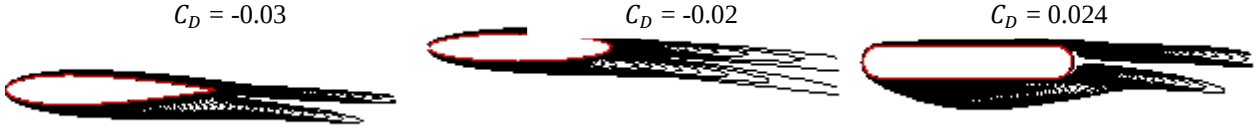

Figure 5-20 Vorticity Contours of NACA0014, Ellipse and Flat Plate at *K* = 0.5

Chapter 6: AIRFOIL SHAPE EFFECT ON AERODYNAMIC PERFORMANCE AND SYSTEMETIC INVESTIGATION OF REDUCED FREQUENCY AT REYNOLDS NUMBER (Re) OF 1000

The effect of airfoil shape on the aerodynamic performance of plunging airfoils in laminar regime has also been investigated. Computations have been performed at a Reynolds number of 1000 and at reduced frequencies of K = 2.0, 1.0 and 0.5 respectively. All other parameters are kept same as mentioned in the validation studies. Flow has been assumed as laminar.

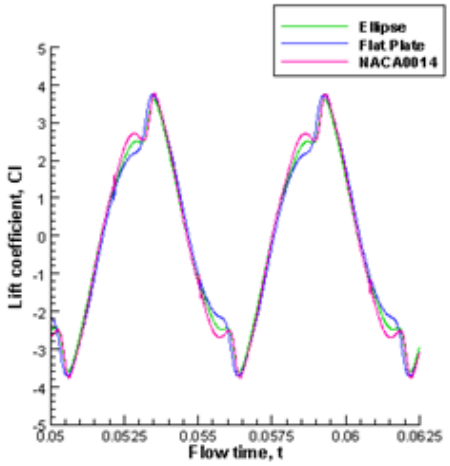

Figure 6-1 C_L Vs time plot at Re = 1000, K = 2.0

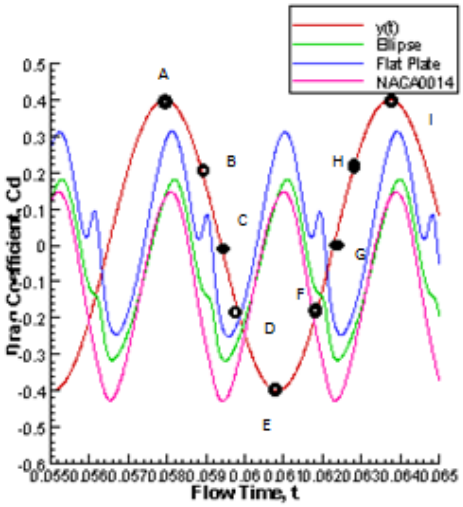

Figure 6-2 C_DVs time plot at Re = 1000, K = 2.0

Figure 6-1and 6-2 represents lift and drag histories at reduced frequency of *K*=2.0. It is observed that the behavior of C_L and C_D is sinusoidal. The plots of C_L are identical for all the three shapes of airfoil whereas the plots of C_D vary for all the three cases. The values of C_{Lmax} is 3.9 and C_{Lmin} is -3.9 for all the three cases. The maximum and minimum values of coefficient of lift and drag are shown in table 6-1.

Table 6-1 Instantaneous maximum and minimum values of coefficient of lift and drag at Re = 1000, *K* = 2.0

Airfoil	Re = 1000, *K*=2.0			
	$C_{L\,max}$	$C_{L\,min}$	$C_{D\,max}$	$C_{D\,min}$
NACA0014	+3.9	-3.9	0.06	-0.7
Ellipse	+3.9	-3.9	0.08	-0.4
Flat Plate	+3.9	-3.9	0.23	-0.22

The mean values of coefficient of drag and lift at Reynolds number of 1000 and reduced frequency *K*=2.0 are represented in table 6-2.

Table 6-2 Mean lift and drag coefficients at *K* = 2.0, *K* = 1.0, *K* = 0.5, Re = 1000

Airfoil	*K* = 2.0		*K* = 1.0		*K* = 0.5	
	$\overline{C_L}$	$\overline{C_D}$	$\overline{C_L}$	$\overline{C_D}$	$\overline{C_L}$	$\overline{C_D}$
NACA0014	0.00	-0.13	0.00	0.03	0.00	0.09
Ellipse	0.00	-0.074	0.00	0.04	0.00	0.10
Flat Plate	0.00	0.032	0.00	0.08	0.00	0.13

Lift and drag histories at reduced frequency *K* =1.0 are represented in figure 6-3 and 6-4. These plots show that the variation of C_L and C_D is sinusoidal. From lift plot, slight difference in the maximum and minimum values of coefficient of lift is observed. Flat plate has a little high maximum and minimum value of lift coefficient as compared to ellipse and

NACA0014. Drag history shows that the difference between the plots of C_D for NACA0014 and ellipse is very less as compared to flat plate which is more toward the positive values of coefficient of drag. The maximum and minimum values of coefficient of lift and drag for all the three cases are given in table 6-3 whereas the mean values of coefficient of lift and drag at *K*=1.0 are represented in table 6-2.

Table 6-3 Instantaneous maximum and minimum values of coefficient of lift and drag at Re = 1000, *K*=1.0

Airfoil	**Re = 1000, *K* = 1.0**			
	$C_{L\,max}$	$C_{L\,min}$	$C_{D\,max}$	$C_{D\,min}$
NACA0014	+1.4	-1.4	0.16	-0.08
Ellipse	+1.3	-1.3	0.195	-0.075
Flat Plate	+1.6	-1.6	0.28	0.01

Figure 6-5 and 6-6 represents the C_L Vs time and C_D Vs time plot at *K* = 0.5. The behavior of C_L and C_D remains sinusoidal as in the case of higher reduced frequencies. C_L Vs time plot depicts that the behavior of C_L variation is quite similar for NACA0014 and ellipse quantitatively as compared to flat plate as it achieves very high positive and negative values of C_L as compared to other two cross sections. Same type of behavior is observed in C_D Vs time plot. The instantaneous variation of coefficient of drag is quite similar for NACA0014 and ellipse as compared to flat plate which is showing very high positive values of maximum lift coefficient. Table 6-4 summarizes the maximum and minimum values of coefficient of lift and drag at reduced frequency *K* = 0.5.

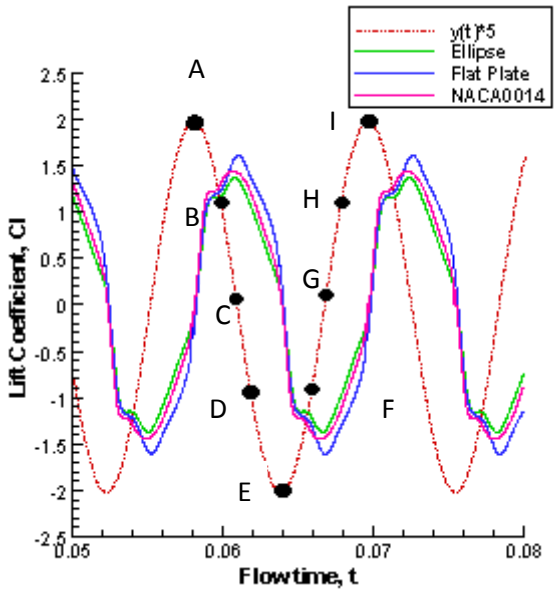

Figure 6-3 C_L Vs time plot at Re = 1000, K = 1.0

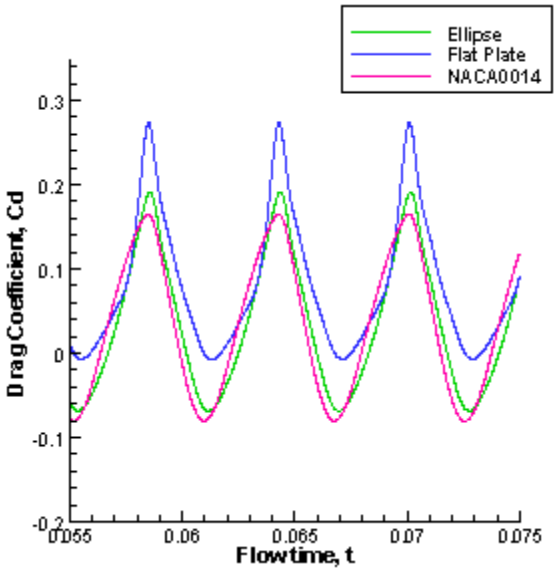

Figure 6-4 C_D Vs time plot at Re = 1000, K = 1.0

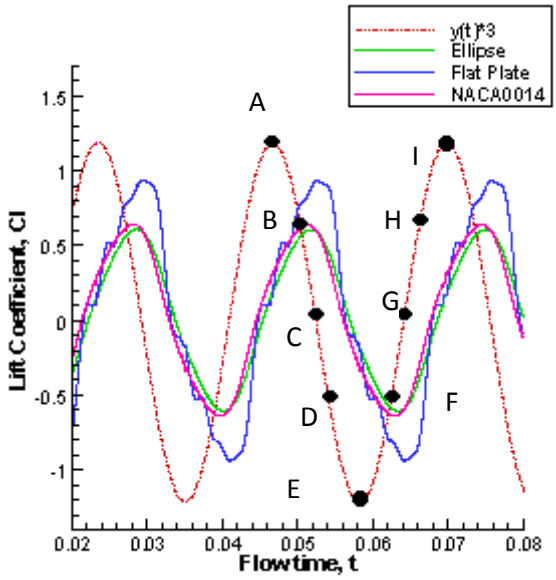

Figure 6-5 C_L Vs time plot at Re = 1000, K = 0.5

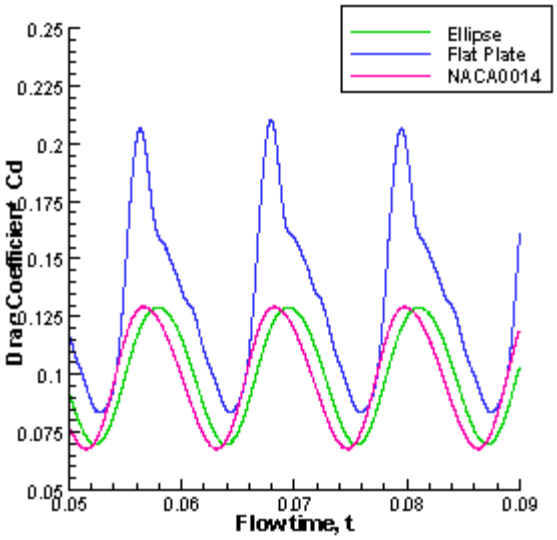

Figure 6-6 C_D Vs time plot at Re = 1000, K = 0.5

Now comparing the present case with that of Reynolds number of 10,000 at K=2.0, it is seen that C_L Vs time plots are quite similar qualitatively as well as quantitatively. C_D Vs time plots for both cases reveals that the maximum and minimum values of coefficient of drag at Re =1000 has been increased as compared with that at Reynolds number of 10,000. Also the mean values of the coefficient of drag show that the thrust produced by all the three shapes of airfoils is decreased. This increase in drag is because the viscous forces dominate the flow at this Reynolds number. Since the viscous forces dominate at low Reynolds number, therefore the contribution of pressure forces in generation of thrust is decreased and contribution of viscous forces is increases as compared with that at Re =10,000 as shown in table 6-4. The difference in the pressure forces of each shape of airfoil is prominent showing that the shape effect is dominant at the given conditions. Although the wake behind the flat plate consists of Reverse Karman Vortex Street, the mean value is still positive showing that drag is produced which is again due to increase in viscous forces as the wake of the airfoil has the secondary effect on drag/thrust generation of the airfoil.

Table 6-4 Pressure and viscous forces for the three shapes of airfoils at Re = 1000 and K = 2.0

Airfoil	**Re = 1000, K = 2.0**					
	Pressure force n	**Viscous force n**	**Total force n**	**Pressure coefficient**	**Viscous coefficient**	**Total coefficient**
NACA0014	-20.62	0.544	-20.08	-0.437	0.0115	-0.425
Ellipse	-14.88	-0.105	-14.988	-0.315	-0.0022	-0.317
Flat Plate	-13.56	1.73	-11.83	-0.287	0.0366	-0.250

At K=1.0 and 0.5, plots of C_L are very similar to that at Re = 10,000. From drag histories, it is seen that at Re = 10,000, difference between the C_D plot for all the three shapes

of airfoils is prominent but at Re = 1000, the plots of ellipse and NACA0014 are very close but difference is prominent as compared to flat plate. Also the mean values of coefficient of drag at Re = 1000 shows that drag is produced by all the airfoils. This is again due to increase in viscous forces at this low Reynolds number. At K = 1.0 and 0.5, unsteady effect is reduced which results in more diffused vortex causing decrease in the thrust produced by the airfoils as the pressure drag increases. Viscous and pressure forces of all the three cases at K = 1.0 and 0.5 are shown in table 6-5 and 6-6 respectively. The values of pressure coefficient for the three cases at this Reynolds number show that the shape effect reduces with the decrease in reduced frequency.

Table 6-5 Pressure and viscous forces for the three shapes of airfoils at Re = 1000 and K = 1.0

Airfoil	**Re = 1000, K = 1.0**					
	Pressure force n	**Viscous force n**	**Total force n**	**Pressure coefficient**	**Viscous coefficient**	**Total coefficient**
NACA0014	-5.67	1.87	-3.79	-0.12	0.039	-0.08
Ellipse	-4.96	1.74	-3.22	-0.10	0.036	-0.06
Flat Plate	-2.49	2.14	-0.34	-0.052	0.045	-0.00

Table 6-6 Pressure and viscous forces for the three shapes of airfoils at Re = 1000 and K = 0.5

Airfoil	**Re = 1000, K = 0.5**					
	Pressure force n	**Viscous force n**	**Total force n**	**Pressure coefficient**	**Viscous coefficient**	**Total coefficient**
NACA0014	-0.0286	3.22	3.20	-0.0006	0.0684	0.0677
Ellipse	-0.219	3.50	3.28	-0.0046	0.0742	0.069
Flat Plate	1.44	2.50	3.948	0.0305	0.05310	0.083

Vorticity plots of the three shapes of airfoils at Reynolds number of 1000 presented in figure 6-7 for reduced frequency of K =2.0 are quite similar when compared with the plots at Reynolds number of 10,000 referred in figure 5-6. This shows that the same amount of lift is produced by all the cross sections at both Reynolds numbers. This is also evident from the lift coefficient plots as shown in figures 5- 2 and 6-1 as these plots are similar qualitatively as well as quantitatively. Same is the case for K=1.0 and 0.5. Lift histories of all the three shapes of airfoils are same at both the reduced frequencies as shown in figure 5-15, 5-17 and 6-3, 6-5 respectively. The vorticity contours are also same showing the similarity in lift produced by all the three cases at both Reynolds number. Only the difference is in the wake of the airfoil which contributes in the thrust/drag produced by the airfoils.

SUMMARY

a) At low Reynolds number of 1000, for high reduced frequencies, all the shapes produces same amount of lift as in case of Re =10,000.
b) Difference in thrust produced by the three shapes of airfoils is also observed at high reduced frequency.
c) Drag coefficient decreases of all the three airfoils as compared to the case of Re =10,000.
d) With the decrease of Reynolds number, viscous forces increase which causes the decrease in thrust production.

NACA0014	ELLIPSE	FLAT PLATE

Position A

C_L = 1.26 ↓ C_D = 0.11	C_L = 1.18↓ C_D = 0.11	C_L = 1.03↓ C_D = 0.26
		

Position B

C_L = 2.53 ↓ C_D = -0.21	C_L = 2.46 ↓ C_D = -0.11	C_L = 2.50 ↓ C_D = 0.03
		

Position C

C_L = 3.64↓ C_D = -0.42	C_L = 3.48↓ C_D = -0.30	C_L = 3.59 ↓ C_D = -0.21
		

Position D

C_L =2.06 ↓ C_D = -0.29	C_L = 1.91 ↓ C_D = -0.24	C_L = 2.16↓ C_D = -0.18
		

NACA0014	ELLIPSE	FLAT PLATE
Position E		
C_L = -1.26 ↑ C_D = 0.11	C_L = -1.17 ↑ C_D = 0.11	C_L = -1.01 ↑ C_D = 0.26
		
Position F		
C_L = -2.51 ↑ C_D = -0.21	C_L = -2.45 ↑ C_D = -0.11	C_L = -2.49↑ C_D = 0.04
		
Position G		
C_L = -3.63↑ C_D = -0.42	C_L = -3.46↑ C_D = -0.30	C_L = -3.56↑ C_D = -0.20
		
Position H		
C_L = -2.04 ↑ C_D = -0.29	C_L = -1.89↑ C_D = -0.23	C_L = -2.13 ↑ C_D = -0.18
		

Figure 6-7 Vorticity contours at Re = 1000, *K* = 2.0

NACA0014	ELLIPSE	FLAT PLATE

Position A

C_L = -0.28 ↓ C_D = 0.13	C_L = 0.12 ↓ C_D = 0.12	C_L = -0.53↓ C_D = 0.14
		

Position B

C_L = 1.31 ↓ C_D = 0.00	C_L = 1.16 ↓ C_D = 0.031	C_L = 1.24↓ C_D = 0.08
		

Position C

C_L = 1.44 ↓ C_D = -0.07	C_L = 1.37 ↓ C_D =- 0.05	C_L = 1.57 ↓ C_D = 0.00
		

Position D

C_L = 1.23 ↓ C_D = -0.03	C_L = 1.09↓ C_D = -0.04	C_L = 1.40 ↓ C_D = 0.00
		

NACA0014	ELLIPSE	FLAT PLATE

Position E

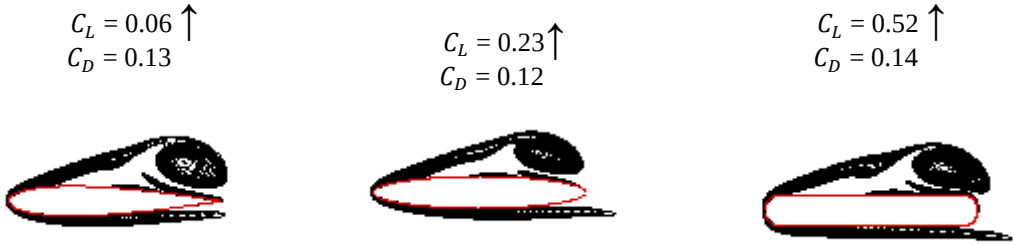

Position F

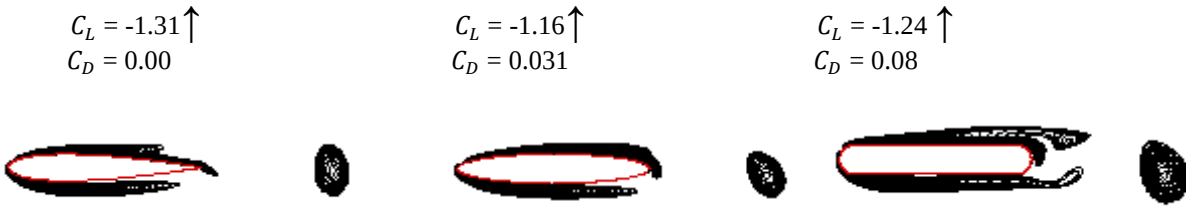

Position G

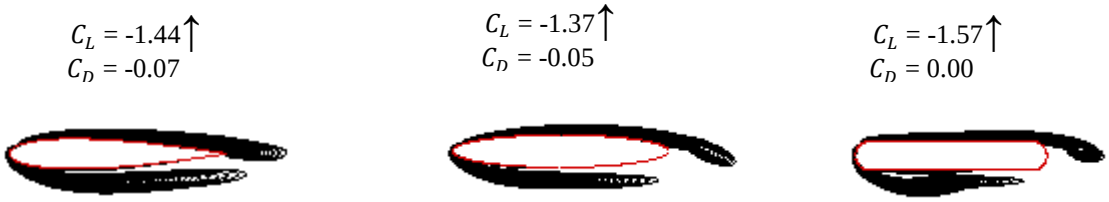

Position H

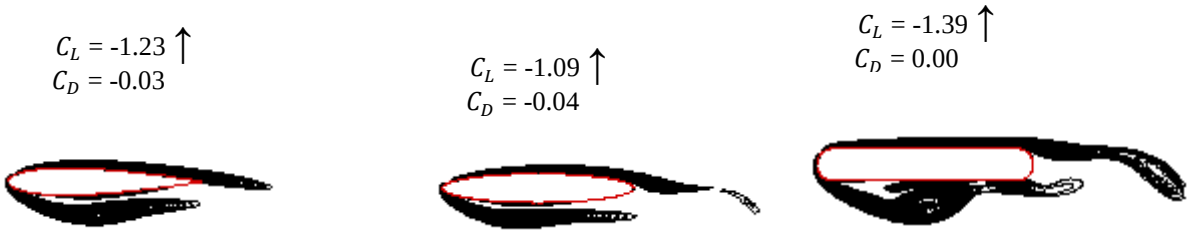

Figure 6-8 Vorticity contours at Re = 1000, *K* = 1.0

NACA0014 **ELLIPSE** **FLAT PLATE**

Position A

C_L = 1.18 ↓
C_D = 0.12

C_L = 1.04↓
C_D = 0.12

C_L = 1.09 ↓
C_D = 0.16

Position B

C_L = 0.61 ↓
C_D = 0.07

C_L = 0.55↓
C_D = 0.08

C_L = 0.76 ↓
C_D = 0.11

Position C

C_L = 0.62 ↓
C_D = 0.069

C_L = 0.60 ↓
C_D = 0.06

C_L = 0.91 ↓
C_D = 0.086

Position D

C_L = 0.38↓
C_D = 0.098

C_L = 0.45 ↓
C_D = 0.08

C_L = 0.88 ↓
C_D = 0.098

NACA0014	ELLIPSE	FLAT PLATE

Position E

C_L = -0.12 ↑ C_D = 0.12	C_L = 0.01 ↑ C_D = 0.12	C_L = 0.028 ↑ C_D = 0.15
		

Position F

C_L = -0.61 ↑ C_D = 0.075	C_L = -0.55 ↑ C_D = 0.08	C_L = -0.76 ↑ C_D = 0.11
		

Position G

C_L = -0.62 ↑ C_D = 0.069	C_L = -0.60 ↑ C_D = 0.06	C_L = -0.91 ↑ C_D = 0.086
		

Position H

C_L = -0.38 ↑ C_D = 0.099	C_L = -0.45 ↑ C_D = 0.08	C_L = -0.87 ↑ C_D = 0.099
		

Figure 6-9 Vorticity contours Re = 1000, *K* = 0.5

Chapter 7: AIRFOIL SHAPE EFFECT ON AERODYNAMIC PERFORMANCE AND SYSTEMETIC INVESTIGATION OF REDUCED FREQUENCY AT REYNOLDS NUMBER, Re = 25,000

Computations have also been carried out at Reynolds number of 25,000 in order to explore the behavior of the three airfoils in pure plunging motion in the fully turbulent flow regime. SA turbulence model has been used in order to capture the turbulence effects at this Reynolds number. Systematic investigation of reduced frequencies has also been carried out at K=2.0, 1.0 and 0.5.

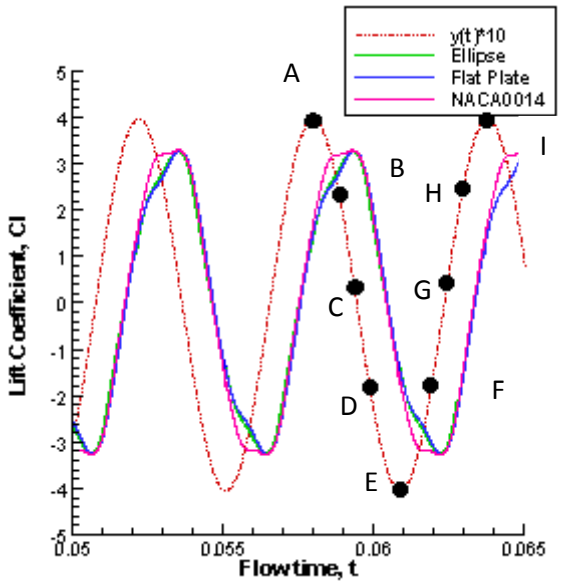

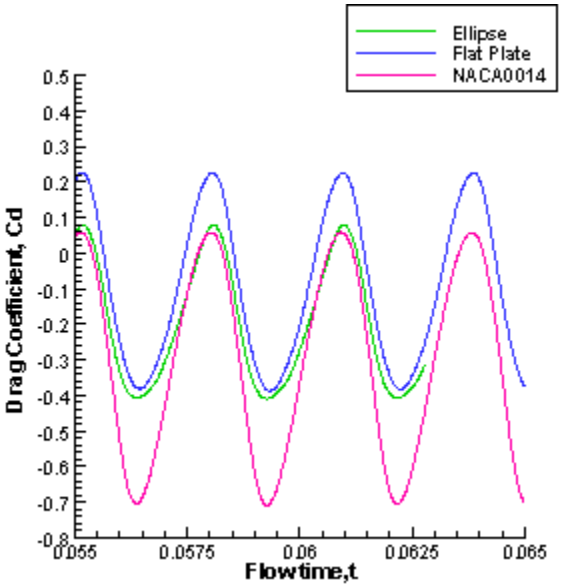

Figure 7-1 Lift Vs time plot at Re = 25,000, *K* = 2.0 **Figure 7-2 Drag Vs time plot at Re = 25,000, *K* = 2.0**

Figure 7-1 and 7-2 shows the variation of coefficient of lift and drag with time for the three shapes of airfoil at reduced frequency of *K*=2.0. These plots depict that the variation of C_L and C_D is sinusoidal as for the previous cases. It is also seen that the variation of C_L is similar for all the three shapes of airfoils but the variation of C_D differs for all the three cases. There is a significant difference in plots of C_D of the three airfoils and NACA0014 is more towards the negative values. The values of C_{Lmax} is 3.2 and C_{Lmin} is -3.2 for all the

three cases. The values of C_{Dmax} and C_{Dmin} for the three cross sections are shown in table 7-1. Mean values of coefficient of lift and drag are tabulated in table 7-2.

Table 7-1 Instantaneous maximum and minimum values of coefficient of lift and drag at Re=25,000, *K*=2.0

Airfoil	Re = 25,000, K = 2.0			
	$C_{L\,max}$	$C_{L\,min}$	$C_{D\,max}$	$C_{D\,min}$
NACA0014	+3.2	-3.2	0.15	-0.42
Ellipse	+3.2	-3.2	0.2	-0.4
Flat Plate	+3.2	-3.2	0.32	-0.37

Table 7-2 Mean lift and drag coefficients at *K* = 2.0, *K* = 1.0, *K* = 0.5, Re = 25,000

Airfoil	K = 2.0		K = 1.0		K = 0.5	
	$\overline{C_L}$	$\overline{C_D}$	$\overline{C_L}$	$\overline{C_D}$	$\overline{C_L}$	$\overline{C_D}$
NACA0014	0.00	-0.30	0.00	-0.10	0.00	-0.02
Ellipse	0.00	-0.19	0.00	-0.06	0.00	-0.01
Flat Plate	0.00	-0.10	0.00	0.00	0.00	0.03

It is observed that the thrust is produced by all the three shapes of airfoils. NACA0014 is producing greatest thrust while the thrust produced by the flat plate is least. This is again due to the reverse Karman vortex street in the wake of airfoil. The generation of thrust at this Reynolds number is again due to the contribution of pressure forces as shown in table 7-3.

Lift and drag histories at reduced frequency of *K*=1.0 are shown in figure 7-3 and 7-4. Variation of C_L and C_D is sinusoidal. C_L Vs time plot depicts that the behavior of NACA0014 and ellipse is almost similar whereas the flat plate has slightly high value of

C_{Lmax} that is +1.7 and C_{Lmin} has a value of -1.7. Drag history shows that the difference between the plots of the coefficient of drag is very prominent even at this low reduced frequency at Re=25,000. The trend of variation of coefficient of drag for the three cross sections is similar to the behavior of the airfoils at reduced frequency of *K*=2.0 that is the plot of NACA0014 is more towards the negative values. The values of C_{Dmin} has been increased and C_{Dmax} has been increased in comparison to the values at *K*=2.0. These values are shown in table 7-4.

Table 7-3 Pressure and viscous forces for the three shapes of airfoils at Re = 25,000 and *K* = 2.0

Airfoil	Re = 25,000, *K*=2.0					
	Pressure force n	Viscous force n	Total force n	Pressure coefficient	Viscous coefficient	Total coefficient
NACA0014	-32.77	-0.64	-33.41	-0.69	-0.013	-0.70
Ellipse	-18.93	-0.35	-19.29	-0.40	-0.007	-0.40
Flat Plate	-18.30	0.067	-18.23	-0.38	0.001	-0.38

Table 7-4 Instantaneous maximum and minimum values of coefficient of lift and drag at Re = 25,000, *K* = 1.0

Airfoil	Re = 25,000, *K*=1.0			
	$C_{L\,max}$	$C_{L\,min}$	$C_{D\,max}$	$C_{D\,min}$
NACA0014	+1.7	-1.7	0.04	-0.26
Ellipse	+1.7	-1.7	0.06	-0.18
Flat Plate	+1.7	-1.7	0.1	-0.08

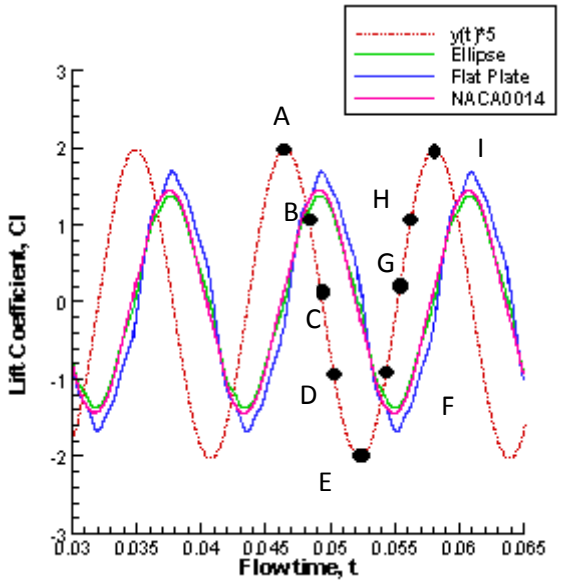

Figure 7-3 Lift Vs time plot at Re = 25,000, *K* = 1.0

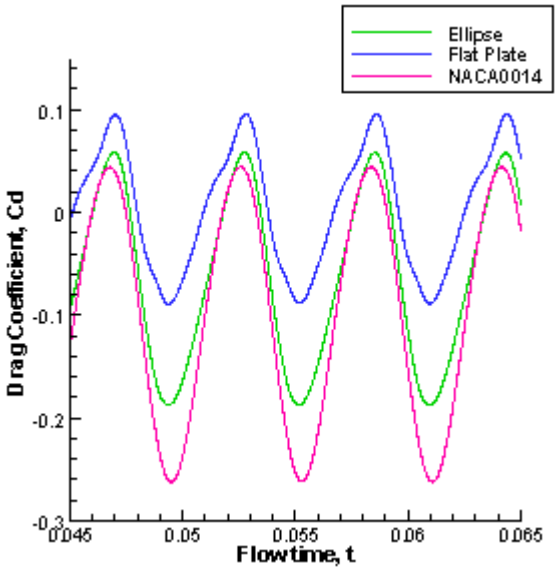

Figure 7-4 Drag Vs time plot at Re = 25,000, *K* = 1.0

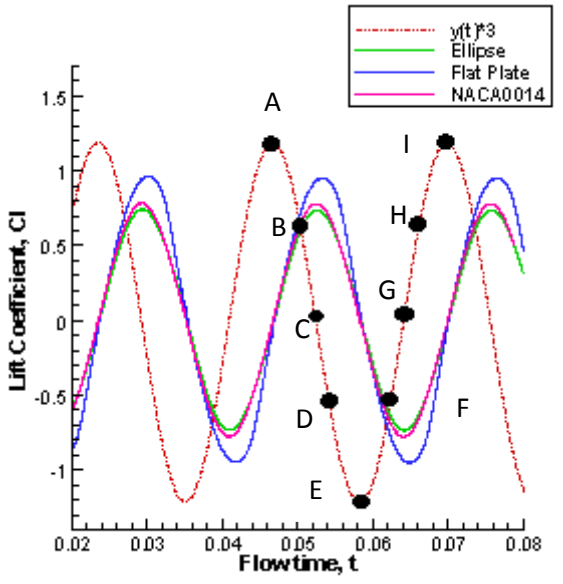

Figure 7-5 Lift Vs time plot at Re = 25,000, *K* = 0.5

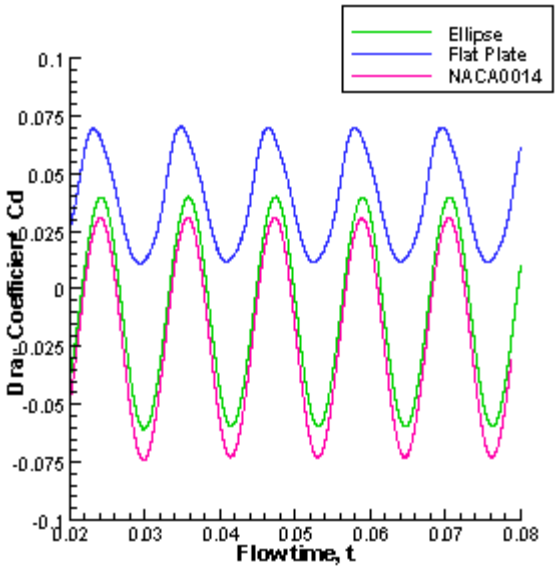

Figure 7-6 Drag Vs time plot at Re = 25,000, *K* = 0.5

Mean values of lift and drag coefficient are shown in table 7-3. Mean values of drag coefficient represents that thrust is produced by NACA0014 and ellipse whereas flat plate is producing zero drag. Now again investigating the contribution of pressure and viscous forces in drag production. The values are shown in table 7-4. These values show that thrust generation is due to pressure forces showing that airfoil shape effect is dominant at Re = 25,000 and K = 1.0.

Table 7-5 Pressure and viscous forces for the three shapes of airfoils at Re = 25,000 and K = 2.0

Airfoil	Re = 25,000, K=1.0					
	Pressure force n	Viscous force n	Total force n	Pressure coefficient	Viscous coefficient	Total coefficient
NACA0014	-12.52	0.15	-12.36	-0.269	0.003	-0.26
Ellipse	-8.98	0.17	-8.81	-0.19	0.003	-0.18
Flat Plate	-4.55	0.35	-4.19	-0.09	0.007	0.08

Table 7-6 Instantaneous maximum and minimum values of coefficient of lift and drag at Re = 25,000, K=0.5

Airfoil	Re = 25,000, K = 0.5			
	$C_{L\,max}$	$C_{L\,min}$	$C_{D\,max}$	$C_{D\,min}$
NACA0014	+1.0	-1.0	0.04	-0.075
Ellipse	+1.0	-1.0	0.04	-0.06
Flat Plate	+1.0	-1.0	0.07	0.02

For K = 0.5, the variation of C_L and C_D remains sinusoidal as shown in figure 7-5 and 7-6. At this reduced frequency, the difference in the variation of coefficient of lift of flat plate becomes more prominent in comparison with the other two cross sections. In case of drag

coefficient, the difference in maximum and minimum values of coefficient of lift of ellipse and NACA0014 has been reduced as the plots of both cross sections comes quite close to each other. The maximum and minimum values of coefficient of lift and drag are shown in table 7-6. Mean values of drag and lift coefficient are shown in table 7-2. It is observed that NACA0014 and ellipse are producing thrust at such a low reduced frequency at the Reynolds number of 25,000.

Comparing the results with that obtained at Re=10,000, it is observed that the trend of variation of both C_L and C_D is quite similar at all reduced frequencies. Plots of C_L are also similar quantitatively for both Reynolds number. Comparing C_D plots reveal that at all reduced frequencies, the plots shifted more towards negative side as the values of C_{Dmax} and C_{Dmin} decreases. This results in decreasing the mean values of coefficient of drag which shows that the greater amount of thrust is produced by the airfoils in this regime.

Now comparing the vorticity plots of all the three shapes of airfoils at Re = 25,000 with the baseline case that is Re = 10,000 at reduced frequency of K = 2.0. The vorticity contours of the three shapes of the airfoils are identical as shown in figure 5-5 and 7-7 which shows that same amount of lift is produced by all the three cross sections at both Reynolds number. This is also evident from lift plots in figures 5-3 and 7-1 as the variation of lift coefficient for both Reynolds numbers is similar qualitatively as well as quantitatively. The vorticity plots also remains same for K = 1.0 and 0.5 for the two Reynolds numbers that is a large vortex is seen in case of flat plate as compared to other two cross sections for both Reynolds number for K = 1.0 which shows that the value of coefficient of lift should increase for flat plate as compared to ellipse and NACA0014. This increase in the value of lift coefficient is also prominent in the lift coefficient plots of both Reynolds numbers as shown in figure 5-7 and 7-3 respectively. Similarly, for K = 0.5, vorticity contours of all the three

shapes of airfoils represented in figure 5-12 and 7-9 shows that the unsteady effect is reduced very much and flow separation is a little bit prominent only for flat plate showing that the high lift is produced by this cross section as compared to the other two cases at both Reynolds number. Same is evident from the lift plots of both Reynolds numbers as shown in figure 5-9 and 7-5 respectively.

SUMMARY

a) Plots of coefficient of lift remains same showing that the same amount of lift is produced by all the shapes at K=2.0 as in the case of Re =10,000.

b) Difference in drag is observed for all the three airfoils at all reduced frequencies

c) Drag coefficient becomes more negative as compared to the case of Re = 10,000 at all reduced frequencies.

d) Thrust increases with the increase of Reynolds number because forces decrease with the increase of Reynolds number.

NACA0014	ELLIPSE	FLAT PLATE

Position A

C_L = 1.28↓ C_D = 0.041	C_L = 1.09↓ C_D = 0.047	C_L = 1.15↓ C_D = 0.20
		

Position B

C_L = 3.20↓ C_D = -0.51	C_L = 2.92↓ C_D = -0.33	C_L = 2.83↓ C_D = -0.25
		

Position C

C_L = 3.28↓ C_D = -0.69	C_L = 3.24↓ C_D = -0.40	C_L = 3.27↓ C_D = -0.38
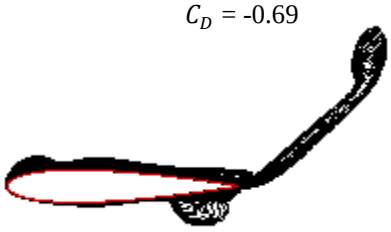		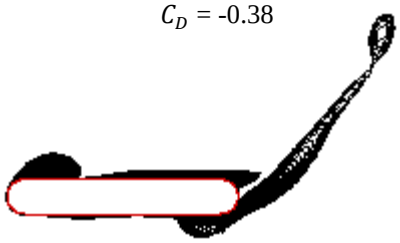

Position D

C_L = 2.35↓ C_D = -0.44	C_L = 2.03↓ C_D = -0.30	C_L = 2.38↓ C_D = -0.24
		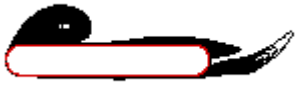

NACA0014	ELLIPSE	FLAT PLATE

Position E

C_L = -1.28 ↑ C_D = 0.042	C_L = -1.09 ↑ C_D = 0.048	C_L = -1.13 ↑ C_D = 0.20
		

Position F

C_L = -3.18 ↑ C_D = -0.51	C_L = -2.92 ↑ C_D = -0.33	C_L = -2.82 ↑ C_D = -0.25
		

Position G

C_L = -3.26 ↑ C_D = -0.69	C_L = -3.23 ↑ C_D = -0.40	C_L = -3.25 ↑ C_D = -0.37
		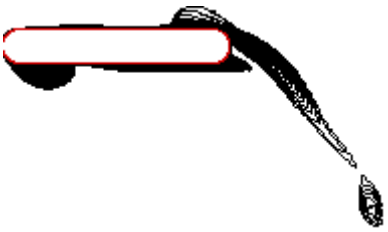

Position H

C_L = -2.33↑ C_D = -0.44	C_L = -1.97↑ C_D = -0.3	C_L = -2.29↑ C_D = -0.233
		

Figure 7-7 Vorticity contours at Re=25,000, *K* = 2.0

NACA0014	ELLIPSE	FLAT PLATE

Position A

C_L = 0.076 ↓ C_D = 0.028	C_L = -0.088↓ C_D = 0.027	C_L = -0.42 ↓ C_D = 0.05
		

Position B

C_L = 1.30 ↓ C_D = -0.13	C_L = 1.16 ↓ C_D = -0.10	C_L = 1.30↓ C_D = -0.03
		

Position C

C_L = 1.43 ↓ C_D = -0.25	C_L = 1.36 ↓ C_D = -0.18	C_L = 1.67 ↓ C_D = -0.08
		

Position D

C_L = 1.18 ↓ C_D = -0.21	C_L = 1.13 ↓ C_D = -0.14	C_L = 1.42 ↓ C_D = -0.05
		

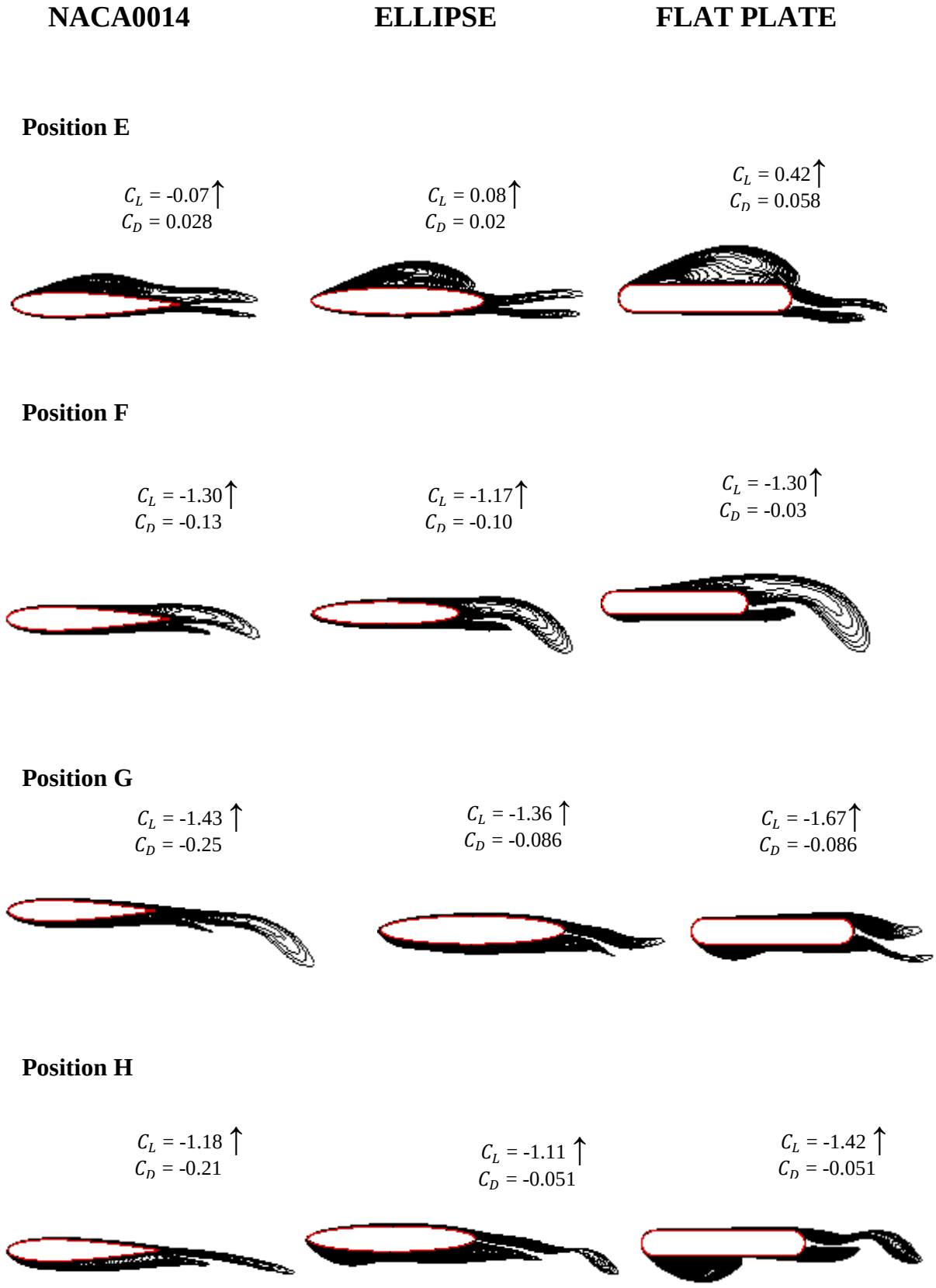

Figure 7-8 Vorticity contours at Re=25,000, *K*=1.0

NACA0014	ELLIPSE	FLAT PLATE

Position A

C_L = 0.80 ↓ C_D = 0.02	C_L = 0.76↓ C_D = 0.032	C_L = 0.81↓ C_D = 0.07
		

Position B

C_L = 0.62↓ C_D = -0.02	C_L = 0.58↓ C_D = -0.01	C_L = 0.69↓ C_D = 0.02
		

Position C

C_L = 0.77↓ C_D = -0.06	C_L = 0.72↓ C_D = -0.053	C_L = 0.91↓ C_D = 0.012
		

Position D

C_L = 0.69↓ C_D = -0.063	C_L = 0.66 ↓ C_D = -0.052	C_L = 0.93 ↓ C_D = 0.018
		

NACA0014	ELLIPSE	FLAT PLATE

Position E

C_L = 0.21↑
C_D = 0.025

C_L = 0.24↑
C_D = 0.032

C_L = 0.29↑
C_D = 0.069

Position F

C_L = -0.62 ↑
C_D = -0.023

C_L = - 0.58↑
C_D = -0.011

C_L = -0.69 ↑
C_D = 0.029

Position G

C_L = -0.77 ↑
C_D = -0.067

C_L = -0.73↑
C_D = -0.053

C_L = -0.91 ↑
C_D = 0.012

Position H

C_L = -0.69↑
C_D = -0.063

C_L = - 0.66↑
C_D = -0.051

C_L = -0.93↑
C_D = 0.019

Figure 7-9 Vorticity contours at Re=25,000, *K*= 0.5

Chapter 8: CONCLUSION

In this research, the plunging motion of three different shapes of airfoils has been investigated numerically by studying the effect of three different parameters one of which was reduced frequency (K) effect; one was Reynolds number effect and the last one airfoil shape effect on the aerodynamic force coefficients. The shapes of airfoils include NACA0014, ellipse and flat plate having same thickness. Now trying to explain clearly the effect of all these parameters independently on the force coefficients as follows

1) First of all explaining the reduced frequency (K) effect on the aerodynamic force coefficients irrespective of Reynolds number and airfoil shape. Computations were carried out at the reduced frequencies of K = 2.0, 1.0 and 0.5. From the results shown in previous chapters it is seen that with the variation of reduced frequency (K), the mean value of coefficient of lift comes out to be zero for all the three shapes of airfoils. It is because the mean attack remains zero for the whole cycle of plunging motion, therefore the lift remains zero. It is also observed that with the increase of reduced frequency (K), more thrust is produced. This is due to the fact that increase in the value of reduced frequency increases the unsteady effect and hence the vertical spacing between the upper and lower row of the vortices in the wake of the airfoil increases which results in more thrust production. At low values of reduced frequencies, the unsteady effect is reduced and the thrust produced by all the airfoils is also reduced as the vertical spacing between the upper and lower row of vortices is also decreased. The variation of coefficient of drag with the reduced frequency (K) is shown in figure 8-1, 8-2 and 8-3 respectively.

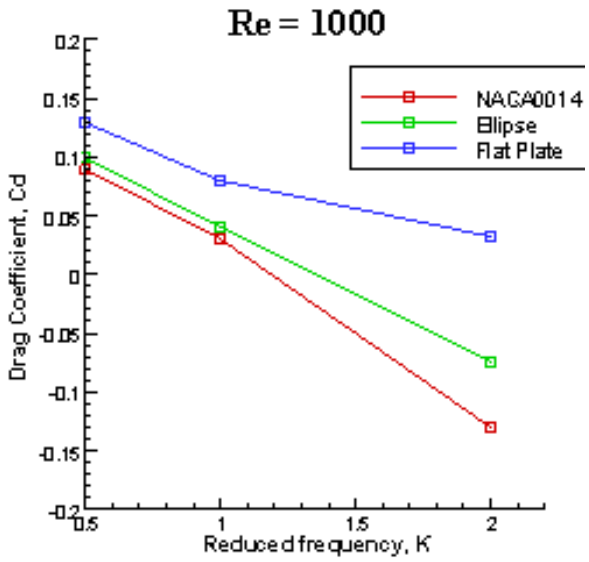

Figure 8-1 C_D Vs K at Re = 1000

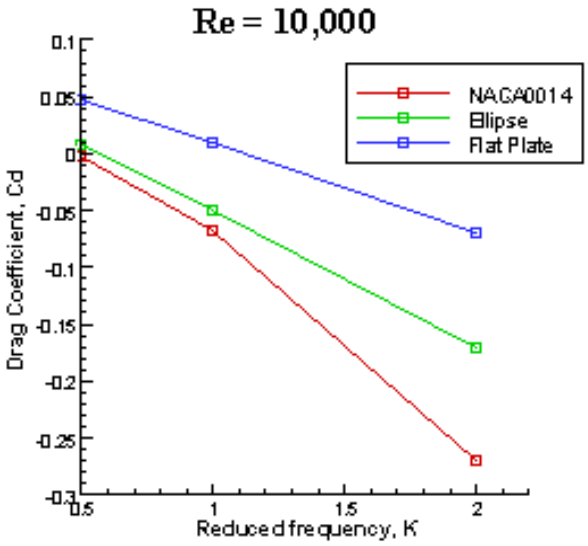

Figure 8-2 C_D Vs K at Re = 10,000

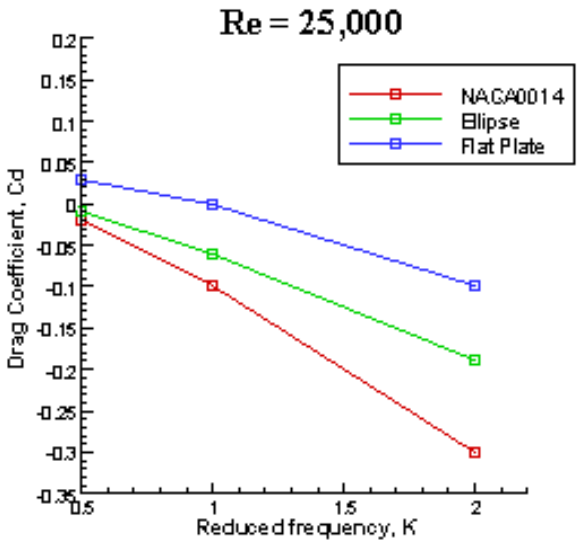

Figure 8-3 C_D Vs K at Re = 25,000

2) Now explaining the effect of Reynolds number irrespective of reduced frequency (K) and shape of airfoil. It is observed that the behavior of coefficient of lift is same at all Reynolds number. Plots of drag coefficient Vs Reynolds number are shown in figures 8-4, 8-5 and 8-6 respectively. It is seen that as the Reynolds number increases, more and more thrust is produced by all the airfoils. The reason behind this increase in thrust is that as the Reynolds number increases, fluid becomes less and less viscous which offers less drag to the airfoils.

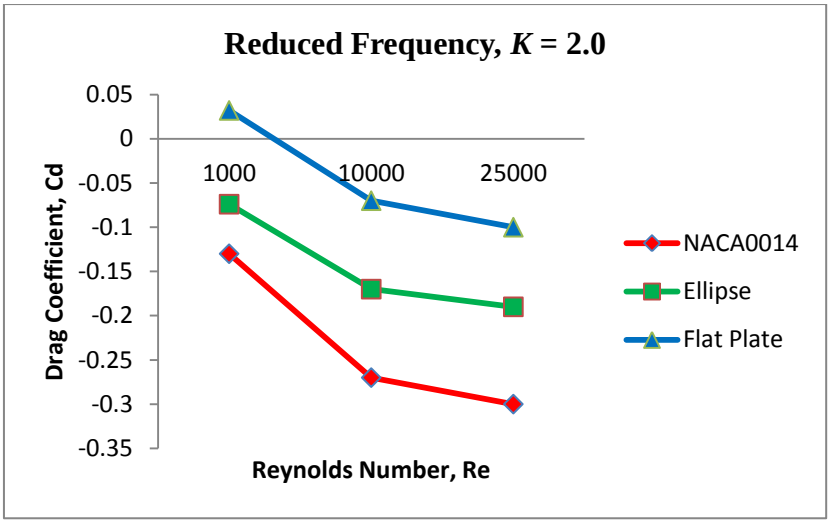

Figure 8-4 C_D Vs Re at K = 2.0

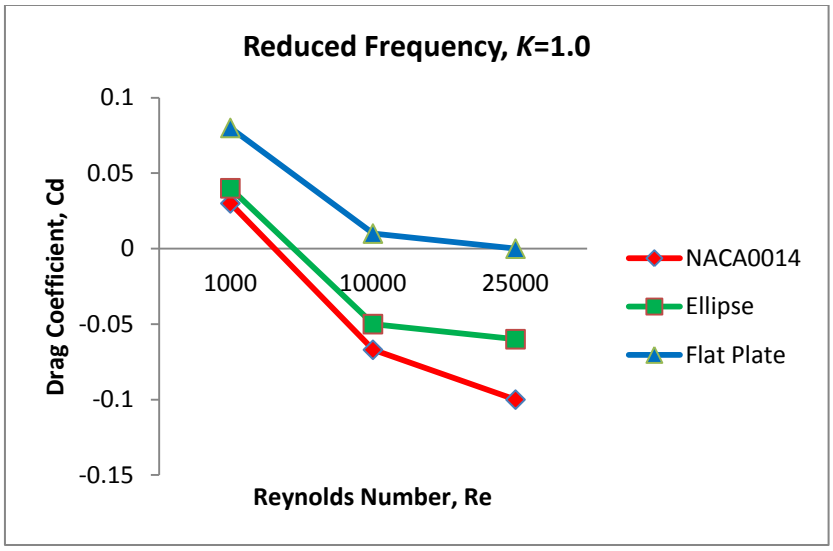

Figure 8-5 C_D Vs Re at K= 1.0

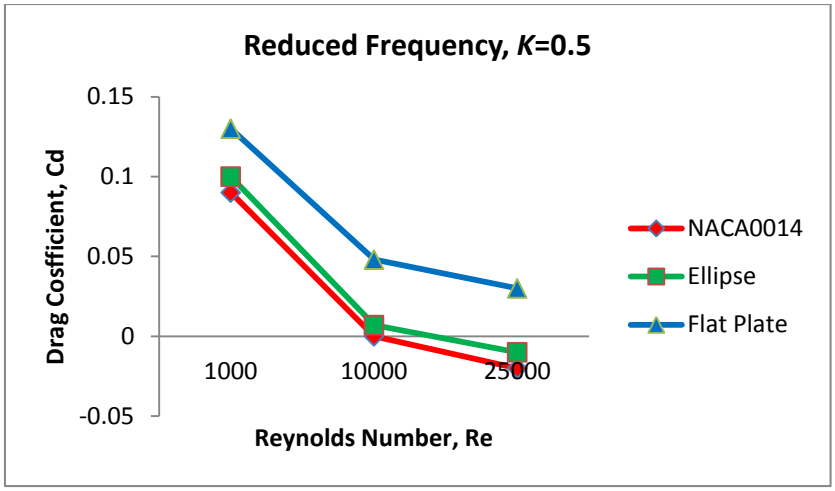

Figure 8-6 C_D Vs Re at K= 0.5

3) As the main aim of the present research is to explore the shape effect at various Reynolds numbers, therefore summarizing the airfoil shape effect on the aerodynamic force coefficients irrespective of the effect of reduced frequency and Reynolds number. It is seen that the more the airfoil has curvature, the more thrust is produced by the airfoil. NACA0014 has more curvature as compared to ellipse and flat plate therefore it produces best thrust as compared to the other two cross sections at all Reynolds numbers which is evident from plots of C_D Vs K and C_D Vs Re .

Hence form the above discussion, it can be concluded that best thrust is produced by the airfoil having more curvature, when there is more unsteadiness that is when the airfoil is made to plunge at high reduced frequency and at high Reynolds number.

APPENDIX - A:

UDF OF PLUNGING MOTION

```
#include"udf.h"
/**************************************************************************
**********
This function defines velocity of center of gravity for pure plunging motion
Equation of Plunging motion is y(t) = hc cosωt----------(Airfoil)
**************************************************************************
**********/

static real velocity=0.0;
DEFINE_CG_MOTION (plung,dt,vel,omega,time,dtime)
{
Thread*t;
face_t*f;
real pi=3.14159;
/*real velocity;*/
real w=1084.375;
real amp=0.0256;

real wt;
/*reset velocities */
NV_S(vel,=,0.0);
NV_S(omega,=,0.0);
if(!Data_Valid_P())
```

```
return;
/* Get the thread pointer for which this motion is defined */
t=DT_THREAD(dt);
/* vel [1] is the vertical plunging velocity */
velocity = -w*amp*sin(w*time);
wt=w*time;
Message ("Time = %f, wt = %f, velocity = %f\n",time,wt,velocity);
}
```

RECOMMENDATIONS/FUTURE WORK:

- To investigate the airfoil shape effect on thrust production in combined (plunging + pitching) motion at various Reynolds numbers and reduced frequencies.
- To investigate the airfoil shape effect on thrust production at an angle of attack in pure plunging motion at various Reynolds numbers and Reduced frequencies.

REFERENCES

[1] Wei Shyy and Michael J. Rycroft, "Aerodynamics of low Reynolds number flyers".

[2] http://en.wikipedia.org/wiki/Micro_air_vehicle visited on 11-10-2011

[3] Ria Malhan, Vinod K. Lakshminarayan, James Baeder, Inderjit Chopra, "Investigation of aerodynamics of rigid flapping wings for mav applications: cfd validation," Presented at the AHS Specialists Conference of the American Helicopter Society, Jan 25-27, Tempe, 2011.

[4] Jing Qian and Zhengke Zhang, "Numerical Study of the Aerodynamic Characteristics of a Plunging Rigid Airfoil with Elastic Trailing-Edge Plate," 20th AIAA Computational Fluid Dynamics Conference, Honolulu, Hawaii, 27 - 30 June 2011.

[5] John Young, "Numerical simulation of the unsteady aerodynamics of flapping airfoils", A thesis submitted for the degree of philosophy, May 2005.

[6] http://www.dicat.unige.it/guerrero/thesischaps/chapter2.pdf visited on 29-11-2011.

[7] Von Karman, T. and Burgers, J.M., "General Aerodynamic Theory," Aerodynamic Theory: A General Review of Progress, edited by W.F. Durand, Vol. 2, Springer, Berlin, 1935.

[8] K.D.Jones and M.F.Platzer, "Numerical computation of flapping-wing propulsion and power extraction", AIAA−97−0826, 35th Aerospace Sciences Meeting & Exhibit January 6−10, 1997 / Reno, NV

[9] R. Knoller, "Die gesetze des luftwiderstands," Flugund Motortechnik, vol. 3, pp. 1–7, 1909.

[10] A. Betz, "Ein beitrag zur erkl¨arung des segelfluges," Zeitschrift f ¨ur Flugtechnik und Motorluftschiffahrt, vol. 3, pp. 269–272, 1912.

[11] Katzmayr, R. (1922), "Effect of periodic changes of angle of attack on behavior of airfoils," NACA TM-147.

[12] M.A. Ashraf, J.C.S. Lai and J. Young, "Numerical Analysis of Flapping Wing Aerodynamics", 16th Australian Fluid Mechanics Conference Crown Plaza, Gold Coast, Australia, 2-7 December 2007.

[13] Heathcote, S., Wang, Z., and Gursul, I., "Effect of Spanwise Flexibility on Flapping Wing Propulsion," 36AIAA Fluid Dynamics Conference and Exhibit, 2006.

[14] Ismail H. Tuncer, Max F. Platzer, "Computational Study of Flapping Airfoil Aerodynamics", Journal of Aircraft Vol. 37, No. 3, May–June 2000.

[15] J.-M. Miao, M.-H. Ho, "Effect of flexure on aerodynamic propulsive efficiency of flapping flexible airfoil", Journal of Fluids and Structures, vol. 22, pp. 401–419, 2006.

[16] Liangyu Zhao and Shuxing Yang, "Influence of Thickness Variation on the Flapping Performance of Symmetric NACA Airfoils in Plunging Motion", Hindawi Publishing Corporation Mathematical Problems in Engineering Volume 2010, Article ID 675462, 19 pages.

[17] M.A. Ashraf, J.Young, J.C.S.Lai, "Reynolds number, thickness and camber effects on flapping airfoil propulsion", Journal of Fluids and Structures, vol. 27, pp. 145–160, 2011.

[18] Joel E. Guerrero, "Effect of Cambering on the Aerodynamic Performance of Heaving Airfoils", Journal of Bionic Engineering. Vol. 6, pp.398–407, 2009.

[19] M. H. Wen, W. R. Hu, and H. Liu, "Thrust Generation Mechanism on Wing Heaving Motion", AIP Conf. Proc. Vol 1376, pp. 190-193, 2011.

[20] J. Young and J.C.S. Lai, "Frequency and Amplitude Effects in the Wake of a Plunging Airfoil", 14th Australasian Fluid Mechanics Conference Adelaide University, Adelaide, Australia 10-14 December 2001

[21] John Young, Joseph C. S. Lai, "On the Aerodynamic Forces of a Plunging Airfoil", Journal of Mechanical Science and Technology 21 (2007) 1388-1397

[22] T. Benkherouf, M.Mekadem, H.Oualli, S.Hanchi, L.Keirsbulck, L.Labraga, "Efficiency of an auto-propelled flapping airfoil", Journal of Fluids and Structures 27 (2011) 552–566.

[23] http://en.wikipedia.org/wiki/NACA_airfoil visited on 04-11-2011

[24] Fluent 6.3 User's guide

[25] http://www.innovative-cfd.com/cfd-grid.html visited on 04-11-2011

[26] http://www.cgl-erlangen.com/downloads/Manual/ch05s04.html visited on 04-11-2011

[27]http://www.howitworksdaily.com/environment/why-does-the-buzz-of-a-fly-and-a-wasp-differ/ visited on 02-05-2012

[28] http://howthingsfly.si.edu/aerodynamics/pressure-drag visited on 02-05-2012

[29] Chunlei Liang, Kui Ou, Sachin Premasuthan, Antony Jameson, Z.J. Wang, "High-order accurate simulations of unsteady flow past plunging and pitching airfoils", Jounal of Computers and fluids.

[30] Anderson , "Fundamentals of aerodynamics".

[31] http://unsworks.unsw.edu.au/fapi/datastream/unsworks:3190/SOURCE01 visited on 10-06-2012

[32] Z. Jane Wang, "Vortex shedding and frequency selection in flapping flight", J. Fluid Mech., vol. 410, pp. 323-341, 2000.

[33] G. C. Lewin and H. Haj-Hariri, "Modeling thrust generation of a two-dimensional heaving airfoil in a viscous flow", J. Fluid Mech., vol. 492, pp. 339–362, 2003.

[34] Lalit K. Chandravanshi, Sunetra Sarkar and Sandip Chajjed, " Study of wake pattern behind an oscillating airfoil", Proceedings of 37th National and 4th International Conference on Fluid mechanics and Fluid Power, , IIT Madras, Chennai, India, Decemeber 16-18 ,2010

[35] John Young, "Numerical Simulation of the unsteady aerodynamics of the flapping airfoils", a thesis submitted for the doctor of philosophy, May 2005.

[36] Meilin Yu, Z. J. Wang, and Hui Hu, "Airfoil Thickness Effects on the Thrust Generation of Plunging Airfoils, Journal Of Aircraft Vol. 49, No. 5, September–October 2012.

[37] Hasan Hizli and D. Funda Kurtulus, "Numerical and experimental analysis of pitching and plunging airfoils in hover," International Micro Air vehicle Conference and Flight Competetion, Braunschweig Germany. 03-06 July 2012.

[38] Wei-Hsin Sun, Jr-Ming Miao, Huai-Te YU, “Low Reynolds number unsteady aerodynamic characteristics of flapping corrugated airfoil,” Seventh International Conference on CFD in the Minerals and Process Industries CSIRO, Melbourne, Australia 9-11 December 2009.

[39] Hiroaki Matsutani, “Unsteady aerodynamics of flapping wings,” 24th international congress of the aeronautical sciences.

[40] G.Y. Oo, K.B. Lua, K.S. Yeo and T.T. Lim, “Wake structures of a heaving airfoil”, 15th Australasian Fluid Mechanics Conference The University of Sydney, Sydney, Australia 13-17 December 2004.

[41] Mahmoud Mekadem, Taha Chettibi, Samir Hanchi, Laurent Keirsbulck, Larbi Labraga, “Kinematic optimization of 2D plunging airfoil motion using the Response Surface Methodology”, Journal of Zhejiang University-Science A (Applied Physics & Engineering) ISSN 1673-565X (Print); ISSN 1862-1775 (Online).

[42] Senthilkumar G and Panchapakesan NR, “Numerical simulation of flapping airfoil using Arbitrary Lagrangian- Eulerian (ALE) method ,” Proceedings of the 37th National & 4th International Conference on Fluid Mechanics and Fluid Power, December 2010.

[43] J. M. Anderson, K. Streitlien, D. S. Barrett and M. S. Triantafyllou, “Oscillating foils of high propulsive efficiency,” J. Fluid Mech., vol. 360, pp. 41-72, 1998.

[44] M. Hafez , A. Shatalov, E. Wahba, “Numerical simulations of incompressible aerodynamic flows using viscous/inviscid interaction procedures”, Comput. Methods Appl. Mech. Engrg., vol. 195, pp. 3110–3127, 2006.

[45] W. Medjroubi, B. Stoevesandt , B. Carmo, J. Peinke, “High-order numerical simulations of the flow around a heaving airfoil,” Computers & Fluids 51 (2011) 68–84.

[46] Wei Shyy and Yongsheng Lian, “Computational investigation of unsteady low-Reynolds number aerodynamics for micro air vehicles,” Final Report: FA9550-06-1-0491.

[47] M.R. Soltani, and F. Rasi Marzabadi, “Effect of Reduced Frequency on the Aerodynamic Behavior of an Airfoil Oscillating in a Plunging Motion”, Transaction B: Mechanical Engineering Vol. 16, No. 1, pp. 40-52.

[48] Antony Jameson, Chunlei Liang, “Unsteady fow past a plunging airfoil”, Workshop on Vortex Dominated Flows, National Institute of Aerospace, June 2009.

[49] Md. Mahbubar Rahman, Md. Mashud Karim and Md. Abdul Alim, “Numerical investigation of unsteady flow past a circular cylinder using 2-d finite volume method, Journal of Naval architecture and marine Engineering, June 2007.

[50] Xue Guang Meng*, Lei Xu and Mao Sun, “Aerodynamic effects of corrugation in flapping insect wings in hovering flight”, The Journal of Experimental Biology 214 , pp 432-444, 2011.

[51] Dong Sun, Huaiyu Wu, Chi Ming Lam, Rong Zhu, “Development of a small air vehicle based on aerodynamic model analysis in the tunnel tests”, Science direct, Mechatronics 16 ,pp.41– 49, 2006.

[52] Jing Qian and Zhengke Zhang, “Numerical Study of the Aerodynamic Characteristics of a Plunging Rigid Airfoil with Elastic Trailing-Edge Plate”, 20th AIAA Computational Fluid Dynamics Conference, June 2011.

[53] Abel Vargas, Rajat Mittal and Haibo Dong, “A computational study of the aerodynamic performance of a dragonfly wing section in gliding flight”, Bioinsp. Biomim., Vol.3 026004 (13pp), 2008.

[54] S. Heathcote, Z.Wang and I.Gursul, “Effect of spanwise flexibility on flapping wing propulsion”, Journal of Fluids and Structures, vol. 24 , pp.183-199, 2008.

[55] Chang-kwon Kang, Hikaru Aono, Pat Trizila, Yeon Baik, Jonathan M. Rausch, Luis Bernal,Michael V. O, and Wei Shyy, “Modeling of Pitching and Plunging Airfoils at Reynolds Number between 1×10^4 and 6×10^4 ,” 27th AIAA Applied Aerodynamics Conference , June 2009.

[56] Jian Tang, Dragos Viieru, and Wei Shyy, “A Study of Aerodynamics of Low Reynolds Number Flexible Airfoils”, 37th AIAA Fluid Dynamics Conference and Exhibit, June 2007.

[57] Xingwei Zhang, Chaoying Zhou, “Numerical investigation on the propulsive efficiency of flapping airfoil with different up-down plunge models”, 27th International congress of the aeronautical sciences, ICAS 2010.

[58] K. Siva Kumar, and Sharanappa V. Sajjan, “ Unsteady Flow past a Flapping Aerofoil”, Transaction on control and mechanical systems, vol.1, no.1, pp. 43-48, May, 2012.

[59] H K Versteeg and W Malalasekera, “An Introduction to Computational Fluid Dynamics, The finite volume method”, Second edition.

[60] Klaus A.Hoffmann and Steve T. Chiang, “Computational Fluid Dynamics”, Fourth Edition, Volume – I.